Coxiella burnetii effector CvpB modulates phosphoinositide metabolism for optimal vacuole development

Eric Martinez, Julie Allombert, Franck Cantet, Anissa Lakhani, Naresh Yandrapalli, Aymeric Neyret, Isobel Norville, Cyril Favard, Delphine Muriaux, Matteo Bonazzi

Coxiella burnetii effector CvpB modulates phosphoinositide metabolism for optimal vacuole development

Eric Martinez[a], Julie Allombert[a], Franck Cantet[a], Anissa Lakhani[a], Naresh Yandrapalli[a], Aymeric Neyret[a], Isobel H. Norville[b], Cyril Favard[a], Delphine Muriaux[a], and Matteo Bonazzi[a,1]

[a]CNRS, Formation de Recherche en Évolution 3689, Centre d'études d'agents Pathogènes et Biotechnologies pour la Santé, Université Montpellier, 34090 Montpellier, France; and [b]Defence Science and Technology Laboratory, Porton Down SP4 0JQ, United Kingdom

Edited by Yasuko Rikihisa, The Ohio State University, Columbus, OH, and approved April 26, 2016 (received for review November 18, 2015)

The Q fever bacterium *Coxiella burnetii* replicates inside host cells within a large *Coxiella*-containing vacuole (CCV) whose biogenesis relies on the Dot/Icm-dependent secretion of bacterial effectors. Several membrane trafficking pathways contribute membranes, proteins, and lipids for CCV biogenesis. These include the endocytic and autophagy pathways, which are characterized by phosphatidylinositol 3-phosphate [PI(3)P]-positive membranes. Here we show that the *C. burnetii* secreted effector *Coxiella* vacuolar protein B (CvpB) binds PI(3)P and phosphatidylserine (PS) on CCVs and early endosomal compartments and perturbs the activity of the phosphatidylinositol 5-kinase PIKfyve to manipulate PI(3)P metabolism. CvpB association to early endosome triggers vacuolation and clustering, leading to the channeling of large PI(3)P-positive membranes to CCVs for vacuole expansion. At CCVs, CvpB binding to early endosome- and autophagy-derived PI(3)P and the concomitant inhibition of PIKfyve favor the association of the autophagosomal machinery to CCVs for optimal homotypic fusion of the *Coxiella*-containing compartments. The importance of manipulating PI(3)P metabolism is highlighted by mutations in *cvpB* resulting in a multivacuolar phenotype, rescuable by gene complementation, indicative of a defect in CCV biogenesis. Using the insect model *Galleria mellonella*, we demonstrate the in vivo relevance of defective CCV biogenesis by highlighting an attenuated virulence phenotype associated with *cvpB* mutations.

Coxiella burnetii | host–pathogen interactions | phosphoinositides

The obligate intracellular bacterium *Coxiella burnetii* is responsible for severe outbreaks of the zoonosis Q fever (1). The primary targets of *Coxiella* are alveolar macrophages; however, bacteria can invade phagocytic and nonphagocytic cells and disseminate to other tissues and organs, such as the liver and heart, giving rise to hepatitis and endocarditis (1). Because of its remarkable infectivity and its environmental stability, *Coxiella* is considered a category B biothreat (2). Upon internalization by phagocytic and nonphagocytic cells, bacteria remain confined within *Coxiella*-containing vacuoles (CCVs), tight-fitting compartments that mature along the endocytic pathway (1). Key to the successful colonization of host cells is the acidification of CCVs, which activates bacterial metabolism and effectors translocation by a Dot/Icm type IV secretion system (3). Bioinformatics analysis identified more than 300 *Coxiella* candidate effectors, a third of which have been validated for secretion (1, 4). Many *Coxiella* effectors remain poorly understood or completely uncharacterized, but it is clear that several of these manipulate host vesicular trafficking, allowing CCVs to intercept and recruit membranes, proteins, and lipids from the endocytic, autophagy, and recycling pathways (4). SNAREs such as VAMP7 and Syntaxin-17 play a key role in this process, mediating the fusion events that lead to the biogenesis of large CCVs that occupy the majority of the host cell cytoplasm (5, 6). Mature CCVs are dynamic acidic compartments (pH 4.8), containing active hydrolases, which *Coxiella* is able to resist, and are positive for markers of late endosomes, lysosomes, and autophagosomes such as vATPase, LAMP1, CathepsinD, CD63, and microtubule-associated protein 1A/1B-light chain 3 (LC3) (7). Many efforts are being focused on the identification and characterization of the *Coxiella* effectors involved in CCV biogenesis, as well as in the identification of the host cell trafficking pathways hijacked by this microbe. It has recently been shown that the *Coxiella* effector *Coxiella* vacuolar protein B (CvpB; also referred to as Cig2) is required for CCV homotypic fusion, which seems to be mediated by the autophagy machinery (8, 9). However, the link between CvpB and autophagy remains to be defined.

Phosphoinositides (PIs) are short-lived lipids whose spatiotemporal localization is determined by the activity of specific kinases and phosphatases (10). Their presence dictates the identity of cellular organelles and allows the targeted recruitment and activation of many downstream effectors, making them important signaling hubs for the regulation of cellular functions, including membrane traffic and actin rearrangement. In recent years, PIs have emerged as new targets for a number of intracellular bacterial pathogens (11–13). As for all host/pathogen interactions, the strategies developed by different pathogens to exploit host PIs are extremely diverse. Bacterial effectors may use host PIs as anchors to specific host cell membranes, whereas others have evolved to manipulate their metabolism directly by mimicking eukaryotic kinases or phosphatases or indirectly by enhancing or blocking the activity of host PI-metabolizing enzymes (11–13). The manipulation

Significance

The biogenesis of a replicative vacuole is an essential step of *Coxiella burnetii* infections and involves the hijack of several host membrane trafficking pathways. Here we describe *Coxiella* vacuolar protein B (CvpB) as a *Coxiella* effector that interacts with phosphoinositides on host cell membranes and manipulates phosphatidylinositol 3-phosphate [PI(3)P] metabolism for optimal *Coxiella*-containing vacuole (CCV) development. This is achieved by perturbing the activity of the phosphatidylinositol 5-kinase PIKfyve, leading to an enrichment of PI(3)P on CCV membranes, which is required for the autophagy machinery to mediate CCV homotypic fusion. The importance of this process is highlighted by a homotypic fusion defect between CCVs in cells infected with CvpB *Coxiella* mutants, which translates into an attenuated virulence in the insect model *Galleria mellonella*.

Author contributions: E.M., J.A., C.F., D.M., and M.B. designed research; E.M., J.A., F.C., A.L., N.Y., A.N., I.H.N., and M.B. performed research; E.M., J.A., F.C., N.Y., and M.B. contributed new reagents/analytic tools; E.M., J.A., F.C., A.L., I.H.N., C.F., D.M., and M.B. analyzed data; and E.M. and M.B. wrote the paper.

The authors declare no conflict of interest.

This article is a PNAS Direct Submission.

[1]To whom correspondence should be addressed. Email: matteo.bonazzi@cpbs.cnrs.fr.

This article contains supporting information online at www.pnas.org/lookup/suppl/doi:10.1073/pnas.1522811113/-/DCSupplemental.

of PI metabolism has pleiotropic downstream effects, mediated by the numerous PI effectors, which are collectively beneficial for the establishment/development of infections.

Building on our recent screen of a *Coxiella* transposon library (14, 15), here we use image-based supervised machine learning to address the mechanisms regulating the fusogenicity of CCVs. We show that the *Coxiella* effector CvpB localizes at CCVs and early endosomes by interacting with phosphatidylinositol 3-phosphate [PI(3)P] and phosphatidylserine (PS). CvpB binding to PI(3)P interferes with the recruitment of the phosphatidylinositol 5-kinase PIKfyve at PI(3)P-positive compartments, thereby preventing PI(3)P phosphorylation to $PI(3,5)P_2$. This allows CvpB to play a dual role in CCV biogenesis during infections. At early endosomes, CvpB leads to the appearance of large PI(3)P-positive compartments that interact and fuse with CCVs for vacuole expansion. At CCVs, CvpB binding to PI(3)P incoming from early endosomes and autophagosomes, and the concomitant inhibition of PIKfyve, is essential to recruit and stabilize components of the autophagy machinery to mediate CCV homotypic fusion. The significance of this process is highlighted by six independent transposon insertions in *cvpB* resulting in a multivacuolar phenotype, with *Coxiella* replicating within isolated CCVs that fail to coalesce into a single vacuole. The *cvpB*::Tn multivacuolar phenotype can be rescued by gene complementation or by inhibiting the phosphatidylinositol 5-kinase PIKfyve, provided that the autophagy machinery is functional. Importantly, despite the lack of an intracellular replication phenotype, *cvpB* mutation attenuates *Coxiella* virulence in the insect model *Galleria mellonella*, demonstrating an important role of CCV biogenesis for *Coxiella* pathogenesis.

Results

Identification of *Coxiella* Factors Involved in CCV Biogenesis Using Image-Based Supervised Machine Learning. In the context of a multiparametric high-content screen of a *Coxiella* transposon mutant library, we have recently reported the seemingly multivacuolar phenotype associated with a transposon insertion in the *dot/icm* gene *icmS* (14). The *Legionella pneumophila* IcmS homolog is a chaperone that mediates the translocation of specific effectors (16, 17), suggesting that *Coxiella* IcmS may regulate the translocation of effectors involved in the homotypic fusion of CCVs. This phenotype was further investigated by challenging Vero cells for 6 d with the *Coxiella* control transposon mutant *Tn1832* [which carries an intergenic transposon insertion and phenocopies WT *Coxiella* (14)] or the *icmS*::Tn mutant and analyzing the morphology of CCVs by fluorescence microscopy. Cells infected with *Tn1832* displayed large CCVs positive for the lysosomal marker LAMP1 and the autophagosomal marker LC3 (*SI Appendix*, Fig. S1 *A* and *B*, *Top*). Conversely, *Coxiella icmS*::Tn replicated within clusters of small LAMP1-positive, but LC3-negative, compartments (*SI Appendix*, Fig. S1 *A* and *B*, *Bottom*). EM confirmed that cells infected with *Tn1832* presented large *Coxiella*-filled vacuoles (*SI Appendix*, Fig. S1*C*, *Left*), as opposed to *icmS*::Tn-infected cells (*SI Appendix*, Fig. S1*C*, *Right*), which presented several tight-fitting vacuoles enclosing few bacteria. To determine whether the multivacuolar phenotype results from the defective secretion of *Coxiella* effectors involved in CCV homotypic fusion, we used image-based supervised machine learning to mine the database generated during the screen of our *Coxiella* transposon library (14) and identify transposon insertions resulting in multivacuolar phenotypes. Among others, this approach identified the *icmS*::Tn mutant as well as all six transposon insertions in *cvpB* (CBU_0021; *SI Appendix*, Fig. S2*A*) previously identified in our screen as affecting the size of intracellular *Coxiella* colonies (14) and recently reported as important for the homotypic fusion of CCVs (8). The axenic and intracellular replication of six independent *cvpB* transposon mutants (*Tn1146*, *Tn396*, *Tn239*, *Tn170*, *Tn2579*, and *Tn2032*) was thus analyzed. When inoculated in the axenic medium acidified citrate cysteine medium-2 (ACCM-2) and allowed to grow for 6 d, *cvpB* mutants replicated with kinetics comparable to those of *Tn1832* (*SI Appendix*, Fig. S2*B*). However, when used to challenge epithelial cell lines (Vero, HeLa, U2OS, or A431), *cvpB* mutants consistently displayed a marked multivacuolar phenotype, with *Coxiella* replicating within clusters of three or more LAMP1-positive CCVs (*SI Appendix*, Fig. S2*C*). The number and size of *Coxiella* CCVs within a cluster varied depending on the cell line: Vero and A431 cells infected with the *cvpB* mutants presented a higher number of relatively small CCVs; these were fewer but larger in HeLa cells, and U2OS cells displayed an intermediate phenotype. More than 50% of cells infected with the *cvpB* mutants presented a multivacuolar phenotype, regardless of the cell line and of the multiplicity of infection (MOI) used for infections (e.g., 100, 10, 1). As previously reported (8), the presence of multiple, average-sized CCVs in cells infected with the *cvpB* transposon mutants did not impact the intracellular replication of *Coxiella* (*SI Appendix*, Fig. S2*D*). *cvpB* encodes an 809-aa protein with a PmrA consensus sequence (18) 102 nt upstream of the start codon and a putative E-block domain (19) at the C terminus (*SI Appendix*, Fig. S2*A*). CvpB translocation was thus assessed by using a β-lactamase secretion assay on U2OS cells challenged with *Coxiella* for 24 and 48 h. β-Lactamase–tagged CvpB was efficiently translocated at both time points (*SI Appendix*, Fig. S3*A*). Conversely, CvpB translocation was abolished by the deletion of its putative E-block or by a transposon insertion in *dotA* (*SI Appendix*, Fig. S3*A*). The efficient expression of all β-lactamase–tagged CvpB constructs was verified by Western blot (*SI Appendix*, Fig. S3*B*). These observations are in agreement with the recently reported translocation of CvpB (8, 9).

The *Coxiella cvpB*::Tn Mutant Is Attenuated in the in Vivo Model *G. mellonella*. The in vivo relevance of the CvpB mutation was investigated by using the insect model *G. mellonella* (20). Larvae were injected in the upper right proleg with 10^6 genome equivalents (GE)/mL of WT *Coxiella*, *Tn1832*, or the *cvpB* mutant *Tn1146*, and the survival rate was determined over 10 d. Larvae injected with PBS solution were used as controls. As previously reported (14, 20), *Galleria* larvae were efficiently killed by WT *Coxiella* or *Tn1832*; however, the injection of the *cvpB* mutant strain resulted in the killing of 50% of the larvae over the same time course (*SI Appendix*, Fig. S3*C*). Importantly, taking into account the lack of obvious intracellular replication phenotypes associated with *cvpB* mutations, this attenuation in virulence speaks in favor of an important role of CCV biogenesis for *Coxiella* pathogenesis. The bacterial load in infected larvae was monitored at 96 and 120 h post injection by real-time PCR using the *Coxiella com1* gene. At both time points, *Coxiella* load within infected larvae was significantly affected in the *cvpB* mutation (*SI Appendix*, Fig. S3*D*).

CvpB Mediates Homotypic Fusion of CCVs and Vacuolation. As all six transposon insertions in *cvpB* result in comparable phenotypes, we focused our study on *Tn1146*, which carries the most upstream transposon insertion, 791 nt downstream of the starting codon (14). Southern blot analysis validated the presence of a single transposon insertion in *Tn1146* (hereafter referred to as *cvpB*::Tn; *SI Appendix*, Fig. S3*E*). The *cvpB*::Tn mutation was complemented by using a mini-Tn7 transposon system to express an HA-tagged copy of CvpB under the regulation of an anhydrotetracycline (aTc)-inducible promoter (*cvpB*::Tn-miniTn7:*cvpB*; hereafter referred to as *cvpB*::Tn Comp.). Expression of CvpB by the *Coxiella* complemented strain was assessed in the presence of aTc by Western blot (*SI Appendix*, Fig. S3*F*). U2OS cells were then challenged with the *cvpB*::Tn complemented strain in the presence of aTc to trigger CvpB expression at the time of infection. Expression of CvpB by *cvpB*::Tn Comp. restored the

formation of single, large CCVs (*SI Appendix*, Fig. S2*C*). To confirm that the multivacuolar phenotype was indeed caused by an impairment of fusion between CCVs, U2OS cells were challenged with the control transposon mutant *Tn1832* or the *cvpB*::Tn mutant for 24 h and imaged over 36 h. CCV formation and development was assessed by phase contrast, and *Coxiella* replication was monitored by using the GFP expressed by transposon mutants. Cells infected with *Coxiella Tn1832* displayed large CCVs undergoing fission and fusion events, whereas cells infected with the *cvpB*::Tn mutant gradually formed smaller CCVs, which largely failed to coalesce into single CCVs over time (Movie S1). Next, U2OS cells were challenged with the *cvpB*::Tn complemented strain, and CvpB expression was triggered at the time of infection or 72 h after infection. Induction of CvpB at the moment of infection restored the formation of single, large CCVs (Movie S1). Cells infected with the noninduced complemented strain presented the typical multivacuolar phenotype. This rapidly converted into a single CCV phenotype upon induction of CvpB expression (Movie S2), clearly demonstrating a role for CvpB in CCV homotypic fusion. Interestingly, cells challenged with *Tn1832* or the *cvpB*::Tn complemented strains were characterized by the formation of large peripheral vesicles, which migrated toward the forming CCV (Movie S1). This was never observed in noninfected cells or in cells challenged with the *cvpB*::Tn strain, suggesting that CvpB favors vacuolation (possibly of early endosomes), which may contribute membranes to the forming CCV over the course of the infection.

CvpB Localizes at CCVs and Early Endosomes, Triggering Endosome Enlargement and Clustering. To investigate the intracellular localization of CvpB, the *cvpB*::Tn mutation was complemented by using a mini-Tn7 transposon system to express a 4xHA-tagged copy of CvpB under the regulation of an aTc-inducible promoter (*cvpB*::Tn 4xHA*cvpB*). The *Coxiella dotA*::Tn mutant (14) was transformed with the same construct as negative control (*dotA*::Tn 4xHA-*cvpB*). U2OS cells were then challenged with the *Coxiella cvpB*::Tn or *dotA*::Tn strains complemented with 4xHA-tagged CvpB in the presence or absence of aTc. Cells were processed for immunofluorescence at different time points postinfection, and an anti-HA antibody was used to reveal the intracellular localization of CvpB. The translocated effector was more efficiently observed at 24 h post infection and mainly labeled CCVs. However, CvpB was also detected as spots scattered throughout the cytoplasm of infected cells (Fig. 1*A*). Labeling was absent in cells challenged with the noninduced *cvpB*::Tn 4xHA*cvpB* strain or the induced *dotA*::Tn 4xHA-*cvpB* strain (Fig. 1*A*). The particular immunofluorescence protocol used to visualize 4xHA-CvpB during infection did not allow the labeling of other intracellular proteins. We thus optimized the codons in the *cvpB* ORF to facilitate expression in eukaryotic cells and generated CvpB constructs carrying HA, FLAG, or mCherry tags at the carboxyl-terminal end of the protein to visualize CvpB upon ectopic expression. Ectopically expressed CvpB decorated LAMP1-positive CCVs in cells infected with the *Coxiella* transposon mutant *Tn1832* (Fig. 1*B*). Confirming our initial observations, CvpB also labeled vesicular structures clustered around CCVs or scattered throughout the cytoplasm of infected cells (Fig. 1*B*), which were LAMP1-negative. Membrane localization was never observed when cells were transfected with plasmids carrying the tags alone.

The nature of CvpB-labeled vesicles was then characterized in noninfected cells. CvpB localized at large vacuolar structures as well as peripheral clusters of smaller vesicles in U2OS cells transfected with HA-FLAG or mCherry-tagged CvpB (Fig. 1*C*, *Left* and *Top Right*). CvpB-HA–transfected U2OS cells were also processed for immuno-EM and analyzed at the ultrastructural level (Fig. 1*C*, *Bottom Right*), confirming CvpB localization at large vacuoles and clusters of smaller vacuoles (Fig. 1*C*, *Bottom*

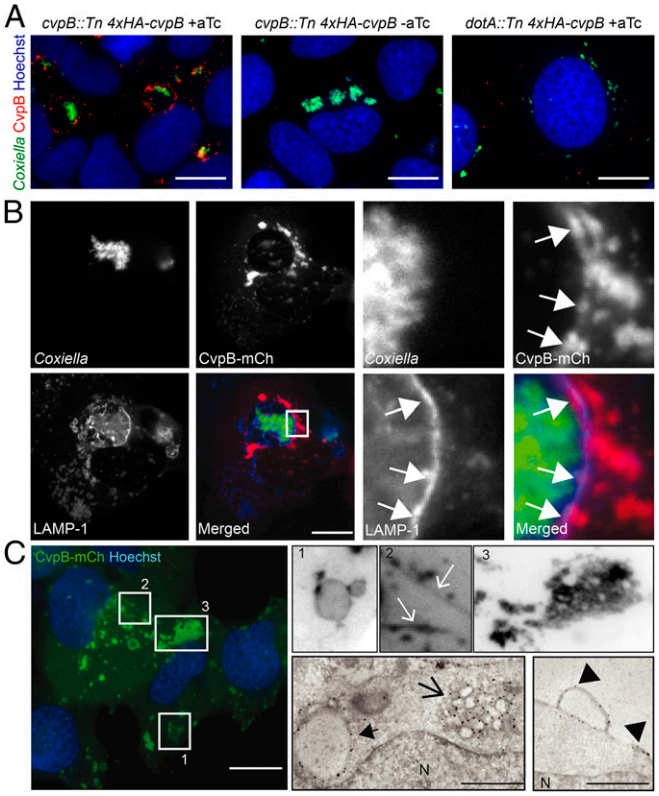

Fig. 1. CvpB localizes at host membranes in *Coxiella*-infected and noninfected cells. (*A*) U2OS cells were challenged with *cvpB*::Tn 4xHA*cvpB* in the presence (*Left*) or absence (*Middle*) of aTc or with *dotA*::Tn 4xHA-*cvpB* in the presence of aTc (*Right*). Cells were fixed 24 h post infection, and translocated CvpB was labeled by using an anti-HA antibody (red), bacteria were visualized using GFP (green), and host cell nuclei were visualized using Hoechst 33258 (blue). (*B*) U2OS cells were infected for 3 d with *Coxiella Tn1832* and transfected with pLVX-CvpB-mCherry. At 12 h post transfection, cells were fixed, and *Coxiella* colonies, CvpB, and LAMP1 were detected by using green fluorescence (green), mCherry fluorescence (red), and anti-LAMP1 coupled to Alexa Fluor 647 (blue), respectively. White arrows indicate discrete regions of the *Coxiella* vacuole where CvpB and LAMP1 colocalize. (*C*, *Left* and *Top Right*) U2OS cells transiently transfected with pLVX-CvpB-mCherry (green) were fixed and labeled with Hoechst 33258 (blue). CvpB is found on large vacuolar structures (*1*), tubules (*2*), and peripheral clusters of smaller vesicles (*3*). (*Insets*) Images shown converted to inverted grayscale. (*C*, *Bottom Right*) U2OS cells transiently transfected with CvpB-HA were fixed and processed for immuno-EM with the HA tag labeled using Nanogold particles. CvpB could be detected in clusters of small vesicles (arrow), enlarged vesicles (filled arrow), or plasma membrane protrusions (arrowheads). (Scale bars: *A*–*C*, *Left* and *Top Right*, 10 μm; *C*, *Bottom Right*, 1 μm).

Middle). Ultrastructural analysis also revealed a clear plasma membrane localization of CvpB that was elusive at the fluorescence level (Fig. 1*C*, *Bottom Right*). Immunogold labeling of CvpB at the plasma membrane was concentrated at microdomains and membrane protrusions. Nontransfected or HA-transfected cells did not present large vacuoles or clusters of small vacuoles. The presence of markers of intracellular compartments at CvpB-induced vacuoles was then assessed. As expected, CvpB-induced vesicles were negative for the lysosomal marker LAMP1 (Fig. 2*A*). It has been suggested that CvpB may be involved in recruiting autophagosomes to forming CCVs (8). We therefore compared CvpB localization with that of the autophagosomal marker LC3. U2OS cells transfected with CvpB-mCherry and LC3C-GFP (Fig. 2*B*) or LC3B-GFP were mock treated or incubated with chloroquine for 3 h before fixation. CvpB was never found colocalizing with either autophagy marker

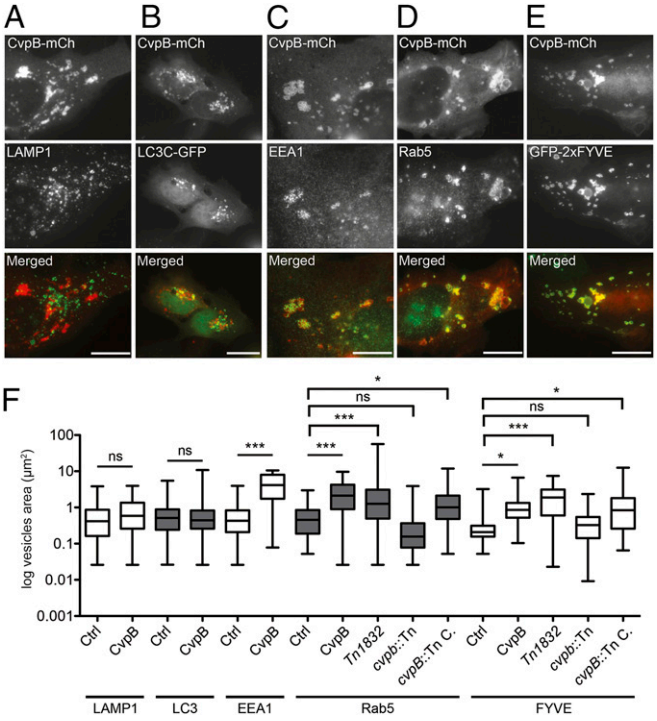

Fig. 2. CvpB colocalizes with early endosome markers triggering their clustering and enlargement. U2OS (*A*–*D*) or U2OS GFP-2xFYVE (*E*) transiently transfected with pLVX-CvpB-mCherry (red) and LC3C-GFP (*B*) were fixed and labeled with anti-LAMP1 (*A*), anti-EEA1 (*C*), or anti-Rab5 (*D*) coupled to Alexa Fluor 488 (green). (Scale bars: 10 μm.) (*F*) The median area of 100 vesicles was calculated in cells transfected with pLVX-mCherry (Ctrl) or pLVX-CvpB-mCherry (CvpB) and in cells infected with *Coxiella Tn1832*, the *cvpB*::Tn mutant, or its complemented strain (*cvpB*::Tn C.; $***P < 0.0001$, $*P < 0.05$; ns, not significant, one-way ANOVA, Bonferroni's multiple comparison test).

in any of the aforementioned conditions (Fig. 2*B*). On the contrary, CvpB vesicles were positive for the early endosomal markers EEA1 (Fig. 2*C*), Rab5 (Fig. 2*D*), and the PI(3)P probe GFP-2xFYVE (Fig. 2*E*). Of note, CvpB expression triggered a significant increase in the size of early endosomes compared with cells expressing mCherry alone (Fig. 2*F*). Late endosome and autophagosome morphology was unaffected by CvpB expression (Fig. 2*F*). These findings indicate that CvpB specifically targets CCVs and early endosomal compartments and is capable of triggering endosome swelling and clustering.

CvpB Binds PI(3)P and PS. The remarkable colocalization between CvpB and the 2xFYVE probe prompted us to determine whether CvpB localization at CCVs and early endosomes might be dictated by direct binding of PI(3)P on host cell membranes. We thus generated a GST-tagged CvpB construct and used the purified recombinant protein in a PIP Strip assay (Fig. 3*A*). Purified GST was used as a control and did not interact with any lipid spotted on the PIP Strips (*SI Appendix*, Fig. S3*G*). Conversely, GST-CvpB bound to monophosphorylated PIs [with a preferential binding to PI(3)P] and with PS (Fig. 3*A*). CvpB binding to PIs was further analyzed by using a PIP array, which confirmed the preferential binding of the *Coxiella* effector to PI(3)P (Fig. 3*B*). CvpB binding to PI(3)P was consistent with the colocalization between CvpB and the PI(3)P probe GFP-2xFYVE, whereas the binding to PS was unexpected. U2OS cells were thus cotransfected with CvpB-mCherry and the GFP-tagged C2 domain of lactadherin (GFP-Lact-C2), a specific PS probe. Indeed, CvpB colocalized with the majority of intracellular structures labeled by GFP-Lact-C2 (*SI Appendix*, Fig. S4*A*). CvpB binding to PS and PI(3)P was then validated by using an in vitro cosedimentation assay in which histidine-tagged CvpB was incubated with large unilamellar vesicles (LUVs) of lipid composition matching those found on PIP Strips at concentrations compatible with those observed in intracellular vesicles (21). In agreement with our observations using PIP Strips, CvpB did not associate with LUVs containing 100% phosphatidylcholine (PC; Fig. 3*C*). CvpB interaction with LUVs was triggered by the combination of 30% PS and 70% PC or 2% PI(3)P and 98% PC at LUVs membranes, and was seemingly enhanced by a mixture of 68% PC, 30% PS, and 2% PI(3)P (Fig. 3*C*).

Bioinformatics analysis failed to highlight known lipid-binding domains for CvpB; thus, a mutational analysis of CvpB-mCherry was carried out to identify the domain(s) required for its recruitment on host cell membranes. Incremental C-terminal deletions up to 500 aa of CvpB did not affect the protein colocalization with FYVE-, Rab5-, and EEA1-positive vesicles (Fig. 3*D* and *SI Appendix*, Fig. S5). Further C-terminal deletions completely delocalized CvpB to the cytoplasm (Fig. 3*D* and *SI Appendix*, Fig. S5). Next, incremental deletions from the N terminus of CvpB were generated. The deletion of the first 100 aa was sufficient to delocalize CvpB to the cytoplasm of transfected cells (Fig. 3*D* and *SI Appendix*, Fig. S5), indicating that the membrane-binding domain (MBD) of CvpB is encompassed between amino acids 1 and 500 (Fig. 3*D*). Of note, despite $CvpB_{1–500}$ colocalization with early endosomal markers, cells transfected with $CvpB_{1–500}$ displayed an attenuated vacuolation phenotype (Fig. 3*D* and *SI Appendix*, Fig. S5), suggesting that the C-terminal domain of the protein plays a role in membrane trafficking. In vitro cosedimentation assay with LUVs confirmed these observations. Histidine-tagged $CvpB_{1–500}$ displayed a binding profile comparable to that of the full-length protein, whereas $CvpB_{500–809}$ did not associate to LUVs, regardless of their lipid composition (Fig. 3*C*).

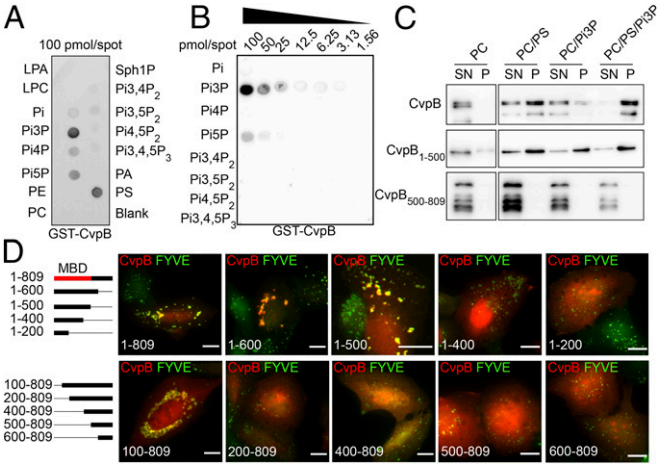

Fig. 3. CvpB interacts with PI3P and PS via its N-terminal domain. Representative protein/lipid overlay assays performed, incubating GST-CvpB with PIP Strips (*A*), whereby several lipids are spotted at 100 pmol per spot, or with PIP Arrays (*B*), whereby PIs are spotted at decreasing concentrations. (*C*) Representative Western blot of cosedimentation assays in which histidine-tagged CvpB (His-CvpB), its 1–500-aa N-terminal domain (His-$CvpB_{1–500}$), or its 500–809-aa C-terminal domain (His-$CvpB_{500–809}$) were incubated with LUVs containing 100% PC, 70% PC and 30% PS (PC/PS), 98% PC and 2% PI(3)P [PC/PI(3)P], or 68% PC, 30% PS, and 2% PI(3)P [PC/PS/PI(3)P]. Following LUV centrifugation, anti-Histidine antibodies were used to detect CvpB in the pellet (P; bound to LUVs) or the supernatant (SN; unbound to LUVs) fraction of samples. (*D*, *Left*) Schematic representation of the CvpB fragments ectopically expressed as mCherry fusion proteins. (*Right*) U2OS GFP-2xFYVE (green) cells were transiently transfected with pLVX-CvpB-mCherry (1–809) or CvpB fragments cloned into pLVX-mCherry (red). (Scale bars: 10 μm.)

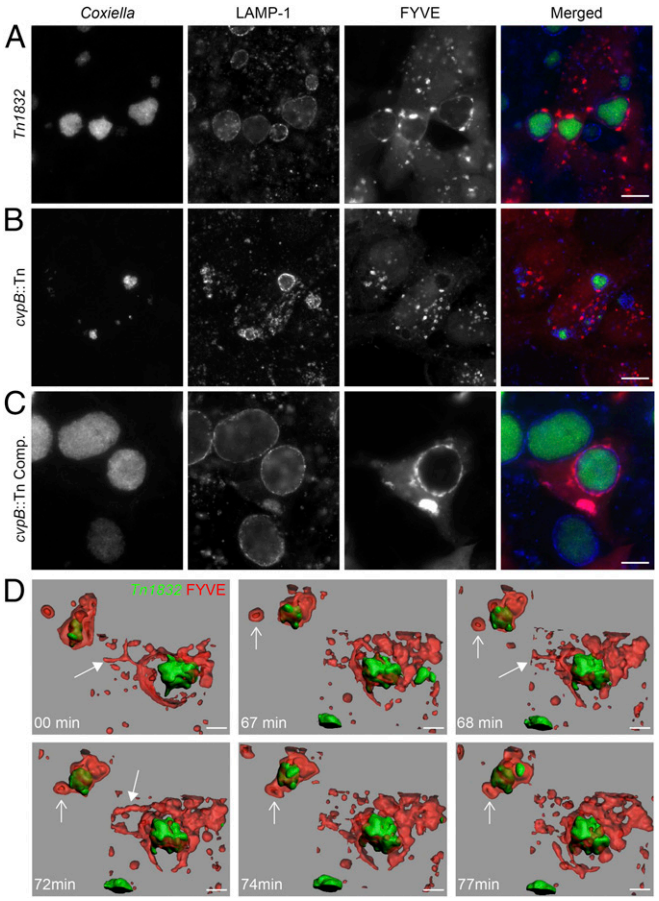

Fig. 4. CvpB induces the presence of PI(3)P at CCV. U2OS mCherry-2xFYVE cells were infected with *Coxiella Tn1832* (*A*), the *cvpB*::Tn mutant (*B*), or the complemented strain (*C*) for 3 d. *Coxiella* colonies, FYVE-positive vesicles, and LAMP1 were detected by using GFP (green), mCherry (red), and an anti-LAMP1 antibody coupled to Alexa Fluor 647 (blue), respectively. (*D*) Representative images from Movie S3 illustrating surface rendering of mCherry-2xFYVE (red) surrounding *Coxiella Tn1832* colonies (green). Filled arrows point at PI(3)P-positive tubules connected with the CCV. Simple arrows follow a representative fusion event between a large PI(3)P-positive vesicle and the PI(3)P-enriched CCV (Movie S3). (Scale bars: *A*–*C*, 10 μm; *D*, 5 μm.)

CvpB Mediates PI(3)P Enrichment of CCVs. To investigate the role of CvpB in CCV biogenesis with respect to its PI(3)P binding property and the colocalization with early endosomal markers, the morphology and dynamics of mCherry-2xFYVE or mCherry-Rab5 were assessed in cells infected with the *Coxiella* control mutant *Tn1832*, the *cvpB*::Tn mutant, or the *cvpB*::Tn complemented strain. In line with our observations in cells ectopically expressing CvpB, cells infected with *Coxiella Tn1832* or the *cvpB*::Tn complemented strain presented large FYVE- and Rab5-positive vesicles, compared with noninfected cells (Fig. 2*F*), which clustered around LAMP1-positive CCVs (Fig. 4 *A* and *C* and *SI Appendix*, Fig. S6*A*). The size of FYVE- and Rab5-positive compartments was unaltered in cells infected with the *cvpB*::Tn mutant, compared with noninfected cells (Fig. 2*F*), and vesicles were scattered through the cytoplasm of infected cells. In all cases, Rab5 was largely excluded from lysosome-derived CCVs (*SI Appendix*, Fig. S6*A*), indicating that, if early endosome/CCV fusion occurred, early endosomal markers were likely lost as a consequence of endosomal maturation. Interestingly, however, the FYVE domain probe was clearly found colocalizing with LAMP1 at CCVs in a CvpB-dependent manner (Fig. 4 *A*–*C*). This observation suggests that CvpB may alter the metabolism of incoming PI(3)P (either from the endocytic or the autophagy pathways) at CCV membranes. The distribution of early endosomal markers with respect to CCVs was also investigated by using cell fractionation. In line with our observations by fluorescence microscopy, the endosomal markers Rab5 and EEA1 were excluded from fractions containing CCVs generated by *Coxiella* Tn1832 and the *cvpB*::Tn mutant (*SI Appendix*, Fig. S6*B*). Fractions containing CCVs from cells infected with the *cvpB::Tn* complemented strain were mainly concentrated in one fraction, which was also positive for Rab5 and EEA1 (*SI Appendix*, Fig. S6*B*), suggesting that early endosomal markers can be found at CCVs, and enrichment of CCVs in a single fraction may facilitate their detection. However, the possibility that early endosomal markers detected by cell fractionation may originate from vesicles clustered around CCVs cannot be excluded. We then used 4D microscopy to investigate the dynamics of CvpB-triggered PI(3)P-positive vesicles in U2OS cells expressing mCherry-2xFYVE. Live imaging confirmed the presence of large PI(3)P-positive vesicles clustered at CCVs generated by the *Coxiella* control transposon mutant *Tn1832* or the *cvpB*::Tn complemented strain (Fig. 4*D* and Movies S3 and S4). In addition, the FYVE probe clearly defined the contour of CCVs under these conditions. Surface rendering of the acquired time lapses revealed the presence of PI(3)P in large patches, which sometimes completely covered the surface of CCVs (Fig. 4*D* and Movies S3 and S4). A number of PI(3)P-positive tubules also emanated from CCVs and interacted with bystander PI(3)P-positive vesicles, which were captured and merged with CCVs (Fig. 4*D* and Movies S3 and S4). Cells infected with the *cvpB*::Tn mutant presented regular-sized PI(3)P-positive vesicles that did not interact with CCVs (Movie S5). Importantly, these findings correlate with our initial observation of waves of large vesicles formed at the periphery of the cell and migrating toward CCVs (Movie S1).

CvpB Modulates the Intracellular Levels of PI(3)P. Host PIs and their metabolism are known targets of a number of bacterial pathogens; we thus investigated whether *Coxiella* uses CvpB to manipulate pathways controlled by PS and/or PI(3)P. Besides its role as a signaling lipid during apoptosis, it has been reported that PS plays an important role in retrograde traffic from the plasma membrane to the Golgi complex (22). We therefore transfected U2OS cells with mCherry or CvpB-mCherry and monitored retrograde transport by incubating cells with 1 μg/mL FITC-labeled Cholera toxin B subunit (CtxB). After 60 min incubation on ice, cells were washed and CtxB was chased at 37 °C for 30 and 60 min. Further confirming CvpB localization at early endosomes, CtxB was observed partially localizing at CvpB-positive compartments 30 min post internalization (*SI Appendix*, Fig. S4*B*, *Top*). At later time points, however, CtxB trafficked to the Golgi complex unperturbed (*SI Appendix*, Fig. S4*B*, *Bottom*) in control and CvpB-expressing cells (*SI Appendix*, Fig. S4*C*).

We next focused on the interaction of CvpB with PI(3)P. This key signaling phospholipid is primarily produced at the level of early endosomes and autophagosomes by the phosphorylation of phosphatidylinositol in position 3 of the inositol ring, mediated by class II and III PI3Ks (10). U2OS cells expressing GFP-2xFYVE were thus treated with the PI3Ks inhibitors LY294002, Spautin-1, or 3-methyladenine (3-MA) to deplete the majority of PI(3)P and monitor the effects of PI(3)P depletion on the intracellular distribution of CvpB. Upon GFP-2xFYVE relocalization to the cytoplasm, cells were transfected with mCherry alone or with CvpB-mCherry. DMSO-treated cells were used as control. mCherry alone was found in the cytoplasm of DMSO-treated or PI3Ks inhibitor-treated cells (Fig. 5*A*), whereas CvpB-mCherry was observed labeling large vacuoles and clusters of smaller vacuoles in DMSO-treated cells (Fig. 5*B*, *Top*). Interestingly, when CvpB-mCherry was expressed in PI(3)P-depleted cells, the bacterial effector was still observed labeling the same vesicular structures as in control cells

(Fig. 5*B*, *Bottom* and *SI Appendix*, Fig. S7). Surprisingly, these vesicles were also labeled by GFP-2xFYVE, indicating the presence of PI(3)P (Fig. 5*B*, *Bottom* and *SI Appendix*, Fig. S7). The levels of intracellular PI(3)P were calculated as the ratio of GFP-2xFYVE intensity between labeled compartments and the cytoplasm, revealing that CvpB expression restored 60% of the PI(3)P probe on endosomal membranes (Fig. 5*C*). The same results were obtained in cells transfected with CvpB before PI(3)P depletion. Our observations suggest that CvpB may influence the metabolism of PI(3)P in cells infected by *Coxiella*.

CvpB Increases Intracellular Levels of PI(3)P by Perturbing the Activity of the PI 5-Kinase PIKfyve. Increases in the intracellular levels of PI(3)P may result from an increased PI3-kinase activity or an inhibition of PI 5-kinase activity (10). However, the restoration of PI(3)P upon CvpB expression in the presence of several PI3Ks inhibitors seems to rule out the possibility that CvpB modulates PI3Ks activity. By using an in vitro PI3-kinase activity assay, we investigated the possibility that CvpB itself may act as a PI3-kinase. In agreement with the lack of known PI3-kinase domains in the sequence of CvpB, the *Coxiella* effector did not exhibit any kinase activity compared with Vps34, used here as positive control, regardless of the temperature used for the assay or the protein concentration (Fig. 5*D*). We therefore tested the possibility that CvpB perturbs the activity of the PI3 phosphate 5-kinase PIKfyve, which phosphorylates PI(3)P in position 5 of the inositol ring to generate $PI(3,5)P_2$ (10). Indeed, several studies reported an increase of PI(3)P leading to vacuolation in cells where the activity of PIKfyve has been perturbed (23–25). The effects of PIKfyve inhibition on PI(3)P-positive endosomes were then compared with those of CvpB overexpression. U2OS cells expressing GFP-2xFYVE were incubated with the specific PIKfyve inhibitor YM201636 (25) or transfected with CvpB-mCherry. In agreement with our hypothesis, PIKfyve inhibition phenocopied the ectopic expression of CvpB (Fig. 5 *E* and *F*). We thus tested whether inhibiting PIKfyve in cells pretreated with PI3K inhibitors restores PI(3)P on early endosomes, as observed with the ectopic expression of CvpB. U2OS cells expressing GFP-2xFYVE were treated with LY294002, Spautin-1, or 3-MA for 4 h. Upon GFP-2xFYVE relocalization to the cytoplasm, the PIKfyve inhibitor YM201636 was added to the culture medium (in the presence of PI3Ks inhibitors). Indeed, the combined treatment of cells with PI3Ks inhibitors and YM201636 restored PI(3)P on endosomal membranes, as indicated by the reappearance of GFP-2xFYVE on these compartments (Fig. 5 *C* and *G*). PIKfyve and CvpB are both recruited at membranes by interacting with PI(3)P (26), raising the possibility that CvpB perturbs PIKfyve activity by interfering with its recruitment at early endosomes. U2OS cells were transfected with GFP-PIKfyve in combination with mCherry, CvpB-mCherry, $CvpB_{100–809}$-mCherry, $CvpB_{1–400}$-mCherry, and $CvpB_{1–500}$-mCherry. PIKfyve recruitment at membranes was then measured as the number of GFP puncta in transfected cells for each condition. As previously described, control cells presented a large cytoplasmic pool of PIKfyve as well as a number of small puncta, revealing the protein association with endosomal vesicles (24, 27) (Fig. 6 *A* and *D*). The coexpression of PIKfyve with CvpB, significantly reduced the number of GFP puncta (Fig. 6 *B* and *D*), indicating that, indeed, CvpB perturbs PIKfyve association with PI(3)P-positive vesicles. Accordingly, coexpression of PIKfyve with CvpB MBD mutants restored membrane localization of PIKfyve (Fig. 6*D*), indicating that membrane targeting of CvpB is required for PIKfyve perturbation. Finally, coexpression of PIKfyve with $CvpB_{1–500}$-mCherry also restored PIKfyve localization at cell membranes, where it colocalized with CvpB (Fig. 6 *C* and *D*), indicating that CvpB does not outcompete PIKfyve for PI(3)P, and that the C terminus domain of CvpB is involved in blocking PIKfyve access to early endosomes. This is consistent with the attenuated vacuolation phenotype observed with $CvpB_{1–500}$-mCherry described in Fig. 3*D*.

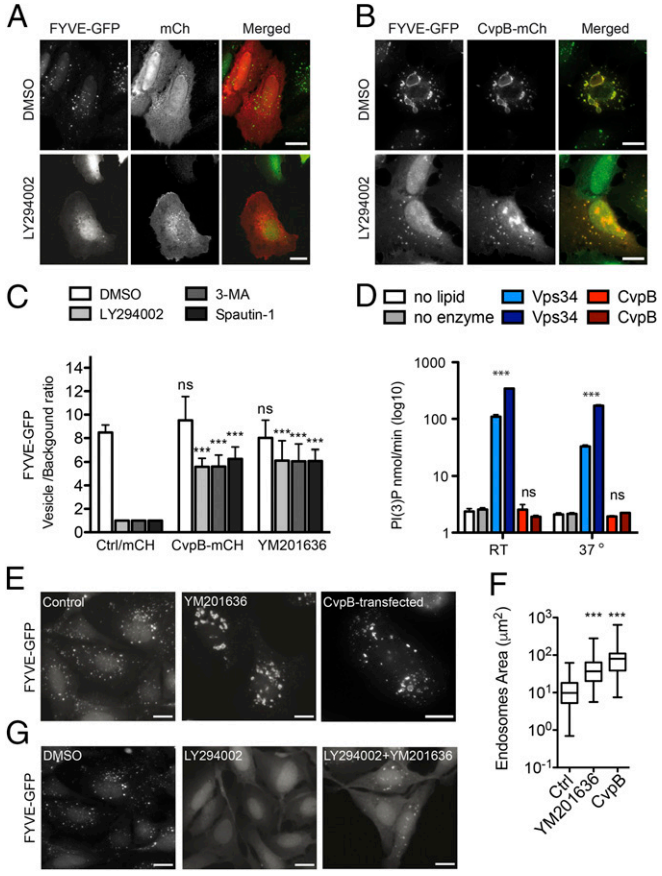

Fig. 5. Ectopic expression of CvpB or PIKfyve inhibition counters the effect of PI 3-kinase inhibitors. U2OS GFP-2xFYVE cells were incubated with DMSO (*Top*) or the PI3-kinase inhibitor LY294002 (*Bottom*) for 4 h and transfected with pLVX-mCherry (*A*) or pLVX-CvpB-mCherry (*B*) for 12 h. The redistribution of the GFP-2xFYVE probe into the cytoplasm was measured as the vesicle-to-background signal ratio of GFP-2xFYVE from 20 treated cells for each condition (*C*) (*SI Appendix*, Fig. S7). (*D*) The PI3-kinase activity of CvpB at 780 nM (light red bars) or 1,560 nM (dark red bars) was measured at room temperature (RT) or 37 °C and compared with no-lipid (white bars) or no-enzyme (gray bars) conditions as negative controls and purified Vps34 at 780 nM (light blue bars) or 1,560 nM (dark blue bars) as positive controls. (*E*) U2OS GFP-2xFYVE cells were incubated with DMSO (control) or YM201636 for 4 h or transfected with pLVX-CvpB-mCherry for 12 h. (*F*) The size of GFP-2xFYVE–positive vesicles in U2OS GFP-2xFYVE cells treated as in *D* was calculated. (*G*) U2OS GFP-2xFYVE cells were incubated with DMSO or the PI3-kinase inhibitor LY294002 for 4 h. The PIKfyve inhibitor YM201636 was then added to cells treated with LY294002, and cells were incubated for 4 h. Values in *C* and *D* are means ± SEM of triplicate experiments (ns, nonsignificant; ***$P < 0.0001$, two-way ANOVA, Bonferroni's multiple comparison test). Values in *F* are calculated from 500 vesicles measured for each condition (***$P < 0.0001$, one-way ANOVA). (Scale bars: 10 μm.)

PIKfyve Inhibition Favors the Recruitment of the Autophagy Machinery to CCVs to Mediate Their Homotypic Fusion. Our observations raised the interesting hypothesis that CvpB perturbs PIKfyve activity to enrich CCVs in PI(3)P for optimal vacuole biogenesis. To test whether PIKfyve inhibition favors CCV biogenesis, U2OS cells were transfected with nontargeting or with three independent PIKfyve-targeting siRNAs (*SI Appendix*, Fig. S8*A*) before challenge with the *Coxiella* control transposon mutant *Tn1832* or the *cvpB*::Tn mutant. Five days postinfection, cells were fixed and the morphology of CCVs labeled by LAMP1 was investigated. CCV development was remarkably enhanced in PIKfyve-depleted cells, with LAMP1-positive vacuoles being

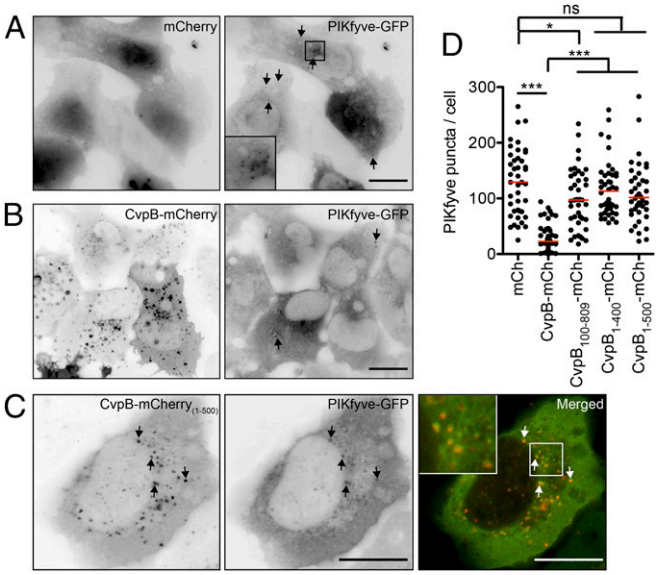

Fig. 6. CvpB perturbs PIKfyve activity by interfering with its recruitment to PI(3)P-positive membranes. U2OS cells were transfected with pGFP-PIKfyve (PIKfyve-GFP) in combination with pLVX-mCherry (*A*), pLVX-CvpB-mCherry (*B*), or pLVX-CvpB$_{100–809}$-mCherry, pLVX-CvpB$_{1–400}$-mCherry, and pLVX-CvpB$_{1–500}$-mCherry (*C*). pLVX-CvpB-mCherry$_{(1–500)}$ (red) and PIKfyve (green) are merged in *C* to illustrate colocalization (arrows and *Inset*). (*D*) The number of PIKfyve-positive puncta (arrows) per cell was calculated by using ICY from 42 cells for each condition. Red bars indicate medians (***$P < 0.0001$; *$P < 0.05$; ns, not significant, one-way ANOVA, Dunnett's multiple comparison test). (Scale bars: 10 μm.)

significantly larger than those developed by control cells infected by *Coxiella Tn1832* (Fig. 7 *A* and *C*). More importantly, the number of cells infected with *Coxiella cvpB*::Tn presenting a multivacuolar phenotype was largely reduced in PIKfyve-depleted cells, with *Coxiella cvpB*::Tn replicating in large CCVs indistinguishable from those generated by *Coxiella Tn1832* (Fig. 7 *B* and *C*). As expected, the multivacuolar phenotype was still observed in cells treated with scrambled siRNA sequences (Fig. 7 *B* and *C*). PIKfyve depletion also restored LC3 labeling on the single CCVs generated by the *cvpB*::Tn mutants (Fig. 7*D*), indicating that PIKfyve inhibition and the concomitant increase in the levels of PI(3)P are functional to the recruitment of the autophagosomal machinery to CCVs. Next, we investigated whether the inhibition of PIKfyve is capable of restoring the single CCV phenotype independently of the autophagy machinery. U2OS cells treated with siRNAs targeting ATG5 or ATG7 (*SI Appendix*, Fig. S8*B*), alone or in combination with siRNAs targeting PIKfyve, were challenged with *Coxiella Tn1832* or the *cvpB::Tn* mutant and analyzed 5 d post infection for the presence of multiple CCVs per cell. Inhibition of autophagy triggered the appearance of a multivacuolar phenotype in cells infected with *Coxiella Tn1832*, as previously described (6) (Fig. 7*C*). Importantly, the combined inhibition of ATG proteins and PIKfyve failed to rescue the multivacuolar phenotype triggered by the inhibition of autophagy (Fig. 7*C*); however, the multiple CCVs per cell were larger, compared with cells interfered for ATG proteins alone (Fig. 7*C*). Accordingly, the same phenotype was observed in cells challenged with the *cvpB::Tn* mutant, where PIKfyve depletion largely failed to rescue the multivacuolar phenotype in absence of a functional autophagy machinery (Fig. 7*C*). In these cells, the inhibition of ATG5 or ATG7 alone had no impact on the multivacuolar phenotype triggered by the *cvpB::Tn* mutant (Fig. 7*C*), suggesting that the CvpB-mediated inhibition of PIKfyve is a prerequisite for CCV expansion and to prime CCV membranes for the recruitment of the autophagy machinery. In turn, autophagy controls homotypic fusion between CCVs. To further define the relative contribution of the endocytic and autophagy pathway to CCV biogenesis with respect to CvpB, U2OS cells treated with siRNAs targeting EEA1 or Rab5 (*SI Appendix*, Fig. S8*B*), alone or in combination with PIKfyve, were challenged with *Coxiella Tn1832* or the *cvpB::Tn* mutant and analyzed 5 d post infection for the presence of multiple CCVs per cell. The inhibition of EEA1 or Rab5 in cells infected with *Coxiella Tn1832* or the *cvpB*::Tn mutant significantly reduced the size of CCVs, but had no effect on the number of CCVs per cell, compared with cells treated with control siRNA sequences (Fig. 7*C*). The combined inhibition of PIKfyve and Rab5 failed to rescue the size of CCVs; however, it partially rescued the multivacuolar phenotype in cells challenged with the *cvpB*::Tn mutant (Fig. 7*C*).

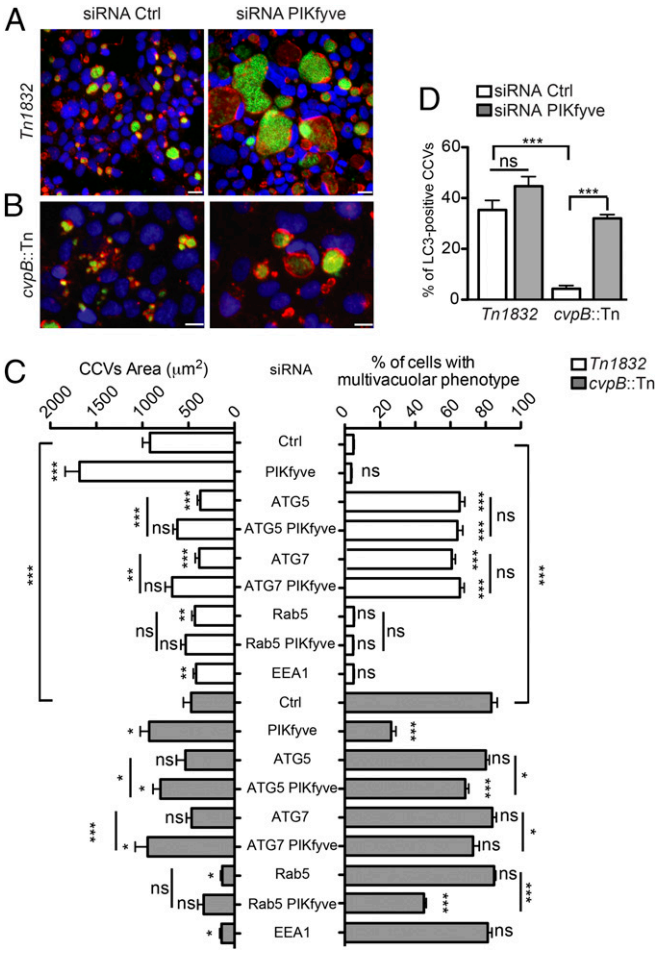

Fig. 7. CvpB-mediated inhibition of PIKfyve promotes homotypic fusion of CCVs via autophagy. U2OS cells were treated with control siRNA (*Left*) or siRNA targeting PIKfyve (*Right*) for 24 h before being challenged with *Coxiella Tn1832* (*A*) or the *cvpB*::Tn mutant (*B*) for 5 d. Cells were then fixed, and LAMP1 and DNA were labeled by using an anti-LAMP1 antibody coupled to Alexa Fluor 555 (red) or Hoechst 33258 (blue), respectively. *Coxiella* colonies were detected by using green Fluorescence (green). (*C*) U2OS cells transfected with the indicated siRNA sequences were challenged with *Coxiella Tn1832* (white bars) or the *cvpB*::Tn mutant (gray bars). The median area of CCVs and the percentage of cells presenting a multivacuolar phenotype (CCVs per cell > 3) were calculated for each condition by using CellProfiler. (*D*) The percentage of CCVs positive for LC3 in cells treated as in *A* and *B* was assessed for each condition. Values are means ± SEM of triplicate experiments in which 200 CCVs or 200 cells were analyzed for each condition (***$P < 0.0001$; **$P < 0.01$; *$P < 0.05$; ns, not significant, one-way ANOVA, Bonferroni's multiple comparison test). (Scale bars: 10 μm.)

Unfortunately, cells did not survive the combined inhibition of EEA1 and PIKfyve. These observations indicate that the endocytic pathway is mainly involved in the initial expansion of CCVs, whereas the autophagy pathway mediates CCV homotypic fusion as previously reported (6).

Discussion

One of the key features of CCVs is their remarkable fusogenicity, which allows these compartments to intercept and merge with the endocytic, autophagy, secretory, and recycling pathways (28–30). To date, however, little is known about the mechanisms responsible for CCV biogenesis as well as the protein and lipid composition of CCVs. In this study, we addressed the fusogenicity of *Coxiella* CCVs, first by describing the multivacuolar phenotype associated with a transposon insertion in the Dot/Icm chaperone IcmS. By using image-based supervised machine learning, we identify *Coxiella* candidate effectors regulating homotypic fusion between CCVs. We have thus identified six independent transposon insertions in *cvpB*, which conferred a multivacuolar phenotype, rescuable by gene complementation. CvpB has been recently identified as a Dot/Icm effector that localizes at CCVs and plays a role in the intracellular development of *Coxiella* (8, 9, 14). A parallel screen of a *Coxiella* transposon library also highlighted the emergence of a multivacuolar phenotype triggered by mutations in *cvpB* (8). The absence of detectable amounts of LC3 on CCVs generated by the *cvpB* mutant suggested a link between CvpB, autophagy, and homotypic fusion between CCVs (8).

By using live imaging in combination with an inducible complementation system, we demonstrate that the multivacuolar phenotype associated with *cvpB* mutations is indeed a result of impaired fusion between CCVs. Importantly, by using the insect model *G. mellonella*, we show that, regardless of the lack of intracellular replication phenotypes observed in cells infected with the *Coxiella cvpB*::Tn mutants, defective CCV biogenesis has in vivo relevance. Intrigued by the remarkable colocalization between CvpB and FYVE domain, a well-established probe for PI(3)P, we used PIP Strip and in vitro cosedimentation with LUV assays to show that the N-terminal domain encompassed between amino acids 1 and 500 allows CvpB binding to PI(3)P- and PS-containing membranes, which is essential to target CvpB to early endosomes. The reported intracellular distribution of PI(3)P on early endosomal membranes and that of PS at the plasma membrane and early endosomes correlated with our results on the subcellular localization of CvpB. Interestingly, ectopically expressed CvpB showed a differential localization in infected vs. noninfected cells. In the absence of infection, CvpB localizes at early endosomes and is excluded from LAMP1-positive lysosomes and autophagosomes, despite the latter sharing a similar lipid composition with early endosomes. On the contrary, in infected cells, the majority of CvpB is recruited to the LAMP1-positive CCV, suggestive of the presence of PI(3)P and/or PS at CCVs. Indeed, we report an unexpected PI(3)P enrichment of *Coxiella* CCVs, which were thus far believed to have mainly lysosomal characteristics. Other early endosomal markers such as EEA1 and Rab5 remain largely undetected at CCVs.

PIs are key players in the regulation of eukaryotic signal transduction, cytoskeleton architecture, and membrane trafficking (10). Specific kinases and phosphatases control their spatial and temporal distribution, allowing a precise and local modulation of essential processes including endocytosis and phagocytosis, membrane traffic, and autophagy (31–33). These processes are commonly manipulated by bacterial pathogens to invade, survive, and replicate within host cells. It is therefore not surprising that PIs and their metabolism have emerged as the target of a growing number of bacterial pathogens (11–13). Bacterial effectors can bind PIs for membrane targeting (34) or acting on PI metabolism, either by means of eukaryotic-like kinases and phosphatases secreted by the pathogen or by modulating the recruitment of host PI-metabolizing enzymes (11, 12). Intravacuolar pathogens subvert PI metabolism to manipulate the lipid profile of their host-derived replicative niche, thus controlling the interactions with the endosomal maturation pathway according to their needs. *Mycobacterium tuberculosis* (35, 36) and *Legionella pneumophila* (37, 38) use effectors to deplete PI(3)P at the surface of their vacuoles to block phagosomal maturation and avoid fusion with degradative compartments. On the contrary, *Salmonella enterica* serovar Typhimurium uses the SPI-1 substrate SopB to maintain elevated levels of PI(3)P at the surface of *Salmonella*-containing vacuoles, favoring their biogenesis (39–41). Based on previous reports, the main source of PI(3)P-positive membranes for CCVs are early endosomes and autophagosomes (4). However, PI(3)P at late endosomes/lysosomes is expected to be further phosphorylated to $PI(3,5)P_2$, by the activity of the PI 5-kinase PIKfyve. Similarly to *Legionella* effectors, CvpB uses PIs for membrane anchoring, apparently using a nonconventional lipid-binding domain as previously reported for the *Legionella* effectors SidC and SidM (42, 43). Similarly to the *Salmonella* effector SopB, *Coxiella* CvpB triggers an increase in PI(3)P levels of infected cells to favor the biogenesis of a spacious replicative compartment (40). CvpB, however, does not possess PI3-kinase activity. Instead, it uses its C-terminal domain to perturb the recruitment of the PI 5-kinase PIKfyve at PI(3)P-positive membranes, thereby interfering with its function and preserving PI(3)P at CCVs. Whether this occurs by steric hindrance or by a yet unidentified catalytic activity of the C-terminal domain of CvpB remains to be elucidated. Accordingly, it has been reported that the genetic, siRNA, or pharmacological-mediated inhibition of PIKfyve is accompanied by an increase in PI(3)P (23–25). PIKfyve inhibition has an important impact on endosomal maturation (23, 24, 44, 45), retrograde traffic (46), and autophagy (47, 48), which collectively result in the formation of large, late endosomal compartments in which the autophagosomal marker LC3 accumulates as a result of the defective fusion with lysosomes. These features are also shared by *Coxiella* CCVs. Accordingly, inhibition of PIKfyve phenocopied the ectopic expression of CvpB, and the depletion of PIKfyve rescued the multivacuolar phenotype in cells infected with the *Coxiella cvpB*::Tn mutant, restoring the formation of large CCVs positive for LAMP1 and LC3.

PI(3)P generated by the autophagy-associated class III PI3-kinase Vps34 is a master regulator of autophagy (49–51), and the PI3-kinase inhibitors used in this study are also commonly used autophagy inhibitors. A significant proportion of CCVs are positive for LC3, indicating that the *Coxiella* replicative compartment intersects the autophagy pathway during maturation. Rather than stimulating autophagy, however, *Coxiella* infections seem to perturb its flux, similarly to what has been described for PIKfyve inhibition (8, 47, 52). The emergence of multivacuolar phenotypes when *Coxiella*-infected cells are silenced for ATG5, ATG12, and the autophagy SNARE Syntaxin-17 (6, 8) demonstrates an important role of autophagy in the homotypic fusion between CCVs. As previously reported (8), we confirm here that *Coxiella cvpB* mutants generate LC3-deficient CCVs. However, the connection between CvpB and the autophagy machinery remained to be defined. CvpB and LC3 localization at distinct intracellular compartments in noninfected cells seems to rule out a direct interaction between CvpB and autophagosomes. Interestingly, however, the presence of LC3 on CCVs generated by the *cvpB*::Tn mutant is rescued, together with the single CCV morphology, by gene complementation or by PIKfyve silencing, indicating that the CvpB-mediated inhibition of PIKfyve is the link between the *Coxiella* effector and the autophagy machinery during CCV biogenesis. PIKfyve inhibition by CvpB, and the concomitant presence of PI(3)P at CCVs, may contribute to stabilize preexisting LC3 at the surface of *Coxiella* vacuoles.

Alternatively, other *Coxiella* effectors may act in response to CvpB to recruit LC3 to CCVs.

In summary, here we show that, similarly to other intracellular bacterial pathogens, *Coxiella* uses effectors to manipulate PI metabolism during infection. Upon translocation, CvpB associates with CCVs and early endosomes by interacting with PI(3)P and PS. There, CvpB exerts a dual function by interfering with the activity of the PI 5-kinase PIKfyve to trigger an increase in the levels of PI(3)P at specific subcellular compartments. At early endosomes, this triggers vacuolation and clustering, which may enhance the delivery of membranes, proteins, and lipids to CCVs for optimal expansion. At CCVs, CvpB perturbation of PIKfyve activity stabilizes the autophagy machinery that mediates homotypic fusion between independent CCVs. Solving the crystal structure of CvpB will provide important insights into the precise molecular mechanism of this remarkable *Coxiella* effector. Four-dimensional microscopy revealed interactions between PI(3)P-positive endosomes and forming CCVs, which become enriched in PI(3)P. The unexpected observation of PI(3)P at CCVs, revealed by the specific probe FYVE, stresses the importance of characterizing the protein as well as lipid composition of the *Coxiella* replicative niche to better understand its biogenesis.

Materials and Methods

Bacterial Strains, Cell Lines, and Growth Conditions. Strains used in this study are listed in *SI Appendix*, Table S1. *Escherichia coli* strains were grown in Luria–Bertani medium supplemented with ampicillin (100 μg/mL), kanamycin (50 μg/mL), or chloramphenicol (30 μg/mL) as appropriate. *C. burnetii* NMII and transposon mutants were grown in ACCM-2 supplemented with kanamycin (340 μg/mL) or chloramphenicol (3 μg/mL) as appropriate in a humidified atmosphere of 5% CO_2 and 2.5% O_2 at 37 °C. U2OS GFP-2xFYVE cells were provided by Tassula Proikas-Cezanne (Eberhard Karls University Tübingen, Tuebingen, Germany). Cells (Vero, HeLa, A431, U2OS, U2OS GFP-2xFYVE, U2OS mCherry-2xFYVE) were routinely maintained in DMEM containing 10% (vol/vol) FCS in a humidified atmosphere of 5% CO_2 at 37 °C. Cell growth medium was supplemented with 600 μg/mL of Geneticin G418 (Gibco) as appropriate. For PI3-kinase inhibition assay, U2OS GFP-2xFYVE cells were incubated at 37 °C, 5% CO_2, with 50 μM LY294002, 10 mM 3-MA, or 10 μM Spautin-1 for a minimum of 4 h. Delocalization of GFP-2xFYVE to the cytoplasm was monitored over time by using an inverted EVOS fluorescence microscope. Where appropriate, after 4 h of treatment with the aforementioned inhibitors, cells were further incubated with 1 μM YM201636 (always in the presence of the PI3-kinase inhibitors) for 4 h to block PIKfyve activity. Alternatively, U2OS GFP-2xFYVE cells were incubated with 1 μM YM201636 alone for 4 h at 37 °C, 5% CO_2, to monitor the effects of PIKfyve inhibition.

Cell Transfection. For the ectopic expression of proteins in mammalian cells, cells were grown to 60% confluence and transfected with JetPEI cationic polymer transfection reagent (Polyplus Transfection) according to the manufacturer's recommendations. Cells were assayed 12–24 h post transfection. For the generation of U2OS mCherry-2xFYVE, cells were grown to 60–80% confluence before being transfected as described earlier. Cells were then incubated at 37 °C and 5% CO_2 for 24–48 h. For enrichment of U2OS mCherry-2xFYVE cells, these were maintained in DMEM supplemented with 10% (vol/vol) FCS and containing 600 μg/mL of Geneticin G418. For gene silencing, U2OS cells were seeded at 2,000 cells per well in black, clear-bottomed, 96-well plates in triplicate and transfected with siRNA oligonucleotides 24 h later by using the RNAiMAX transfection reagent (Thermo Fisher Scientific) according to the manufacturer's recommendations. At 24 h post transfection, cells were challenged with *C. burnetii* transformants (MOI of 100) and further incubated for 5 d. Cells are then fixed and processed for immunofluorescence. In parallel, U2OS cells were cultured in six-well plates and transfected as described earlier. Cell lysates were collected at 24-h intervals during the time course of the experiment, and efficient gene silencing was monitored by Western blot.

Transformation and Axenic Growth of *C. burnetii*. *C. burnetii* strains were transformed with their respective plasmids as described by Martinez et al (14). For routine culture of *C. burnetii* strains, 10^6 GE/mL of bacteria were inoculated in 4 mL ACCM-2 and allowed to grow for 8 d in a humidified atmosphere of 5% CO_2 and 2.5% O_2 at 37 °C. Where needed, 340 μg/mL kanamycin and/or 3 μg/mL chloramphenicol were added as appropriate to bacterial cultures. At the indicated time points, bacterial concentrations were evaluated from 100 μL of cultures by using the PicoGreen (Invitrogen) assay according to the manufacturer's instructions.

Immunofluorescence Staining and Microscopy. Cells were fixed in 3% (wt/vol) paraformaldehyde in PBS solution at room temperature for 30 min or in methanol/acetone (1:1) at −20 °C for 5 min. Samples were then rinsed in PBS solution and incubated in blocking solution (0.5% BSA, 50 mM NH_4Cl in PBS solution, pH 7.4). When appropriate, 0.05% saponin was added to the blocking solution for cell permeabilization. Cells were then incubated with the primary antibodies diluted in blocking solution for 30 min at room temperature, rinsed five times in PBS solution, and further incubated for 30 min with the secondary antibodies diluted in the blocking solution. Fluorescent phalloidin was added to the secondary antibodies to label actin when needed. To visualize translocated 4xHA-tagged CvpB, cells were fixed as previously described in 3% (wt/vol) paraformaldehyde in PBS solution. Then, cells were permeabilized with 0.5% Triton X-100 in PBS solution for 3 min at room temperature. Sample were then rinsed in PBS solution and incubated with blocking solution [0.1% Triton X-100, 5% (wt/vol) milk in PBS solution] for 1 h at room temperature. Cells were then incubated with the anti-HA antibody diluted in the blocking solution for 1h at 37 °C, rinsed five times in PBS solution, and incubated with the secondary antibody for 1 h at 37 °C. For all conditions, coverslips were mounted by using Prolong Gold antifade mounting medium supplemented with Hoechst 33258 for DNA staining. Samples were imaged with a Zeiss Axio Imager Z1 epifluorescence microscope (Carl Zeiss) connected to a CoolSNAP HQ^2 CCD camera (Photometrics). Images were acquired alternatively with 63× or 40× oil immersion objectives and processed with MetaMorph (Universal Imaging). Alternatively, samples were imaged with an ArrayScan VTI Live epifluorescence automated microscope (Cellomics) equipped with an ORCA-ER CCD camera (Hamamatsu). In this case, 25 fields per well were acquired for image analysis. ImageJ, ICY, and CellProfiler software were used for image analysis and quantifications.

PI3K Activity Assay. For the analysis of PI3-kinase activity of CvpB, the class III PI3-kinase kit was used according to the manufacturer's recommendations (K-3000; Echelon Biosciences). Recombinant VPS34 (Sigma) was used as positive control and conditions without enzyme or PI substrate were used as negative controls. The kinase reaction was performed in 10 mM Tris·HCl, pH 7.6, 100 mM NaCl, 1 mM EDTA, 10 mM $MnCl_2$, and 50 μM ATP using 780 nM or 1.56 μM of recombinant protein.

Protein–Lipid Overlay Assay. Purified GST or GST-CvpB was incubated with PIP Strips and PIP Arrays (Molecular Probes) following the manufacturer's recommendations. Briefly, TBS-T/BSA [10 mM Tris·HCl, pH 8, 150 mM NaCl, 0.1% Tween 20, 3% (wt/vol) BSA] was used throughout the assay. PIP Strips and PIP Arrays were first blocked for 1 h in TBS-T/BSA before being incubated with 1 μg/mL of GST or GST-CvpB at 4 °C overnight. Membranes were washed three times with TBS-T/BSA and immunoblotted with anti-GST HRP-conjugated antibodies for 1 h at room temperature. Following three washes with TBS-T/BSA, the membranes were probed with ECL for signal detection.

In Vitro Cosedimentation Assays with LUVs. Binding of histidine-tagged CvpB, $CvpB_{1–500}$, and $CvpB_{500–809}$ to LUVs was determined by cosedimentation assays. LUVs were made with a mixture of egg PC, brain PS, and PI(3)P at different molar ratios (100:0:0, 70:30:0, 98:0:2, or 68:30:2). Lipid mixtures were solubilized in chloroform, dried by evaporation, and resuspended overnight in a solubilizing buffer (150 mM KCl, 0.5 mM EDTA, 20 mM Hepes, pH 7.4) and extruded to obtain 200-nm-diameter LUVs. A constant amount of proteins (8 pmol), full-length CvpB, $CvpB_{1–500}$, or $CvpB_{500–809}$ was incubated for 30 min at room temperature with LUVs in a final volume of 100 μL. Samples were ultracentrifuged for 30 min at 71,000 rpm in a Beckman TLA 100 rotor at 4 °C. Each sample was then divided into a supernatant (SN; 90 μL), containing unbound proteins, and a pellet (P; 10 μL) containing LUV-bound proteins. The pellet P was resuspended in 80 μL of solubilizing buffer. A total of 20 μL of SN or P was analyzed on a 12% SDS/PAGE gel, and proteins were detected by Western blotting by using an anti-histidine antibody.

Antibodies and reagents, plasmids, and primers used in this study are listed in *SI Appendix*. Procedures for plasmid construction, image-based supervised machine learning, β-lactamase translocation assay, *G. mellonella* survival assay, transmission EM, live imaging, protein expression and purification, and cell fractionation are detailed in *SI Appendix*.

ACKNOWLEDGMENTS. The authors thank Dr. Tassula Proikas-Cezanne (International Max Planck Research School, Eberhard Karls University Tuebingen); Prof. Assia Shisheva (Wayne State University); Dr. Kai Wengelnik (CNRS, UMR 5235, DIMNP); Dr. Gunnar Schroeder (Imperial College London); and Bruno Beaumelle, Martine Biard, Lucile Espert, and Fabien Blanchet (CNRS, FRE 3689, CPBS) for providing cell lines, plasmids, and constructs and for scientific discussions. We thank Virginie Georget, Simon Lachambre, and Sylvain DeRossi (Montpellier RIO Imaging-MRI) and Chantal Cazevieille (COMET EM Platform, Montpellier RIO Imaging) for their technical assistance and data analysis and Dr. Mariella Lomma (CHU, Nimes) for critical reading of the manuscript. This work was supported by Agence Nationale de la Recherche (ANR) Grant ANR-14-CE14-0012-01, project AttaQ, ERA-NET Infect-ERA ANR-13-IFEC-0003, project EUGENPATH, and the ATIP-AVENIR programme.

1. van Schaik EJ, Chen C, Mertens K, Weber MM, Samuel JE (2013) Molecular pathogenesis of the obligate intracellular bacterium *Coxiella burnetii*. *Nat Rev Microbiol* 11(8):561–573.
2. Madariaga MG, Rezai K, Trenholme GM, Weinstein RA (2003) Q fever: A biological weapon in your backyard. *Lancet Infect Dis* 3(11):709–721.
3. Newton HJ, McDonough JA, Roy CR (2013) Effector protein translocation by the *Coxiella burnetii* Dot/Icm type IV secretion system requires endocytic maturation of the pathogen-occupied vacuole. *PLoS One* 8(1):e54566–e54569.
4. Moffatt JH, Newton P, Newton HJ (2015) *Coxiella burnetii*: Turning hostility into a home. *Cell Microbiol* 17(5):621–631.
5. Campoy EM, Mansilla ME, Colombo MI (2013) Endocytic SNAREs are involved in optimal *Coxiella burnetii* vacuole development. *Cell Microbiol* 15(6):922–941.
6. McDonough JA, et al. (2012) Host pathways important for Coxiella burnetii infection revealed by genome-wide RNA interference screening. *mBio* 4(1):e00606–12.
7. Kohler LJ, Roy CR (2015) Biogenesis of the lysosome-derived vacuole containing *Coxiella burnetii*. *Microbes Infect* 17(11-12):766–771, 10.1016/j.micinf.2015.08.006.
8. Newton HJ, et al. (2014) A screen of *Coxiella burnetii* mutants reveals important roles for Dot/Icm effectors and host autophagy in vacuole biogenesis. *PLoS Pathog* 10(7): e1004286–e16.
9. Larson CL, et al. (2015) *Coxiella burnetii* effector proteins that localize to the parasitophorous vacuole membrane promote intracellular replication. *Infect Immun* 83(2): 661–670.
10. De Matteis MA, Godi A (2004) PI-loting membrane traffic. *Nat Cell Biol* 6(6):487–492.
11. Weber SS, Ragaz C, Hilbi H (2009) Pathogen trafficking pathways and host phosphoinositide metabolism. *Mol Microbiol* 71(6):1341–1352.
12. Pizarro-Cerdá J, Kühbacher A, Cossart P (2015) Phosphoinositides and host-pathogen interactions. *Biochim Biophys Acta* 1851(6):911–918.
13. Pizarro-Cerdá J, Cossart P (2004) Subversion of phosphoinositide metabolism by intracellular bacterial pathogens. *Nat Cell Biol* 6(11):1026–1033.
14. Martinez E, Cantet F, Fava L, Norville I, Bonazzi M (2014) Identification of OmpA, a *Coxiella burnetii* protein involved in host cell invasion, by multi-phenotypic high-content screening. *PLoS Pathog* 10(3):e1004013–e1004022.
15. Martinez E, Cantet F, Bonazzi M (2015) Generation and multi-phenotypic high-content screening of *Coxiella burnetii* transposon mutants. *J Vis Exp* (99):e52851–e52851.
16. Zusman T, Yerushalmi G, Segal G (2003) Functional similarities between the icm/dot pathogenesis systems of *Coxiella burnetii* and *Legionella pneumophila*. *Infect Immun* 71(7):3714–3723.
17. Ninio S, Zuckman-Cholon DM, Cambronne ED, Roy CR (2005) The *Legionella* IcmS-IcmW protein complex is important for Dot/Icm-mediated protein translocation. *Mol Microbiol* 55(3):912–926.
18. Beare PA, et al. (2014) Essential role for the response regulator PmrA in *Coxiella burnetii* type 4B secretion and colonization of mammalian host cells. *J Bacteriol* 196(11):1925–1940.
19. Lifshitz Z, et al. (2013) Computational modeling and experimental validation of the *Legionella* and *Coxiella* virulence-related type-IVB secretion signal. *Proc Natl Acad Sci USA* 110(8):E707–E715.
20. Norville IH, et al. (2014) *Galleria mellonella* as an alternative model of *Coxiella burnetii* infection. *Microbiology* 160(Pt 6):1175–1181.
21. van Meer G, Voelker DR, Feigenson GW (2008) Membrane lipids: Where they are and how they behave. *Nat Rev Mol Cell Biol* 9(2):112–124.
22. Uchida Y, et al. (2011) Intracellular phosphatidylserine is essential for retrograde membrane traffic through endosomes. *Proc Natl Acad Sci USA* 108(38):15846–15851.
23. Ikonomov OC, Sbrissa D, Shisheva A (2001) Mammalian cell morphology and endocytic membrane homeostasis require enzymatically active phosphoinositide 5-kinase PIKfyve. *J Biol Chem* 276(28):26141–26147.
24. Ikonomov OC, Sbrissa D, Shisheva A (2006) Localized PtdIns 3,5-P2 synthesis to regulate early endosome dynamics and fusion. *Am J Physiol Cell Physiol* 291(2): C393–C404.
25. Jefferies HBJ, et al. (2008) A selective PIKfyve inhibitor blocks PtdIns(3,5)P(2) production and disrupts endomembrane transport and retroviral budding. *EMBO Rep* 9(2):164–170.
26. Sbrissa D, Ikonomov OC, Shisheva A (2002) Phosphatidylinositol 3-phosphate-interacting domains in PIKfyve. Binding specificity and role in PIKfyve.Endomenbrane localization. *J Biol Chem* 277(8):6073–6079.
27. Cabezas A, Pattni K, Stenmak H (2006) Cloning and subcellular localization of a human phosphatidylinositol 3-phosphate 5-kinase, PIKfyve/Fab1. *Gene* 371(1):34–41.
28. Larson CL, Beare PA, Howe D (2013) Coxiella burnetii effector protein subverts clathrin-mediated vesicular trafficking for pathogen vacuole biogenesis. *Proc Natl Acad Sci USA* 110(49):E4770–E4779, 10.1073/pnas.1309195110/-/DCSupplemental.
29. Berón W, Gutierrez MG, Rabinovitch M, Colombo MI (2002) *Coxiella burnetii* localizes in a Rab7-labeled compartment with autophagic characteristics. *Infect Immun* 70(10): 5816–5821.
30. Campoy EM, Zoppino FCM, Colombo MI (2011) The early secretory pathway contributes to the growth of the *Coxiella*-replicative niche. *Infect Immun* 79(1):402–413.
31. Levin R, Grinstein S, Schlam D (2015) Phosphoinositides in phagocytosis and macropinocytosis. *Biochim Biophys Acta* 1851(6):805–823.
32. Simonsen A, Wurmser AE, Emr SD, Stenmark H (2001) The role of phosphoinositides in membrane transport. *Curr Opin Cell Biol* 13(4):485–492.
33. Vicinanza M, Rubinsztein DC (2016) Mirror image phosphoinositides regulate autophagy. *Mol Cell Oncol* 3(2):e1019974, 10.1080/23723556.2015.1019974.
34. Hilbi H, Weber S, Finsel I (2011) Anchors for effectors: Subversion of phosphoinositide lipids by legionella. *Front Microbiol* 2:91.
35. Fratti RA, Chua J, Vergne I, Deretic V (2003) *Mycobacterium tuberculosis* glycosylated phosphatidylinositol causes phagosome maturation arrest. *Proc Natl Acad Sci USA* 100(9):5437–5442.
36. Vergne I, et al. (2005) Mechanism of phagolysosome biogenesis block by viable *Mycobacterium tuberculosis*. *Proc Natl Acad Sci USA* 102(11):4033–4038.
37. Weber S, Wagner M, Hilbi H (2013) Live-cell imaging of phosphoinositide dynamics and membrane architecture during Legionella infection. *mBio* 5(1):e00839–13.
38. Toulabi L, Wu X, Cheng Y, Mao Y (2013) Identification and structural characterization of a *Legionella* phosphoinositide phosphatase. *J Biol Chem* 288(34):24518–24527.
39. Mallo GV, et al. (2008) SopB promotes phosphatidylinositol 3-phosphate formation on *Salmonella* vacuoles by recruiting Rab5 and Vps34. *J Cell Biol* 182(4):741–752.
40. Hernandez LD, Hueffer K, Wenk MR, Galán JE (2004) *Salmonella* modulates vesicular traffic by altering phosphoinositide metabolism. *Science* 304(5678):1805–1807.
41. Scott CC, Cuellar-Mata P, Matsuo T, Davidson HW, Grinstein S (2002) Role of 3-phosphoinositides in the maturation of *Salmonella*-containing vacuoles within host cells. *J Biol Chem* 277(15):12770–12776.
42. Ragaz C, et al. (2008) The *Legionella pneumophila* phosphatidylinositol-4 phosphate-binding type IV substrate SidC recruits endoplasmic reticulum vesicles to a replication-permissive vacuole. *Cell Microbiol* 10(12):2416–2433.
43. Brombacher E, et al. (2009) Rab1 guanine nucleotide exchange factor SidM is a major phosphatidylinositol 4-phosphate-binding effector protein of *Legionella pneumophila*. *J Biol Chem* 284(8):4846–4856.
44. de Lartigue J, et al. (2009) PIKfyve regulation of endosome-linked pathways. *Traffic* 10(7):883–893.
45. Kim GHE, Dayam RM, Prashar A, Terebiznik M, Botelho RJ (2014) PIKfyve inhibition interferes with phagosome and endosome maturation in macrophages. *Traffic* 15(10):1143–1163.
46. Rutherford AC, et al. (2006) The mammalian phosphatidylinositol 3-phosphate 5-kinase (PIKfyve) regulates endosome-to-TGN retrograde transport. *J Cell Sci* 119(pt 19): 3944–3957.
47. Martin S, et al. (2013) Inhibition of PIKfyve by YM-201636 dysregulates autophagy and leads to apoptosis-independent neuronal cell death. *PLoS One* 8(3):e60152–e14.
48. Vicinanza M, et al. (2015) PI(5)P regulates autophagosome biogenesis. *Mol Cell* 57(2): 219–234.
49. Simonsen A, Tooze SA (2009) Coordination of membrane events during autophagy by multiple class III PI3-kinase complexes. *J Cell Biol* 186(6):773–782.
50. Vergne I, Deretic V (2010) The role of PI3P phosphatases in the regulation of autophagy. *FEBS Lett* 584(7):1313–1318.
51. Burman C, Ktistakis NT (2010) Regulation of autophagy by phosphatidylinositol 3-phosphate. *FEBS Lett* 584(7):1302–1312.
52. Winchell CG, Graham JG, Kurten RC, Voth DE (2014) *Coxiella burnetii* type IV secretion-dependent recruitment of macrophage autophagosomes. *Infect Immun* 82(6): 2229–2238.

Supporting Information

Martinez et al. 10.1073/pnas.1522811113

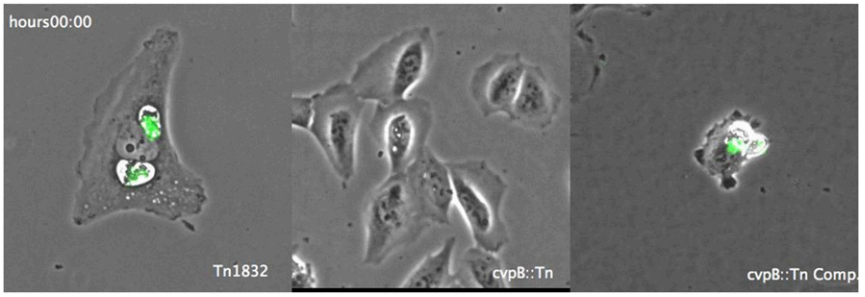

Movie S1. U2OS cells were challenged with the *Coxiella* control transposon mutant *Tn1832* (*Left*), the *cvpB*::Tn mutant (*Middle*), or the *cvpB*::Tn complemented strain (in the presence of aTc; *Right*) for 3 d before imaging. Images were acquired every 10 min for 32 h in the phase-contrast and GFP channels.

Movie S1

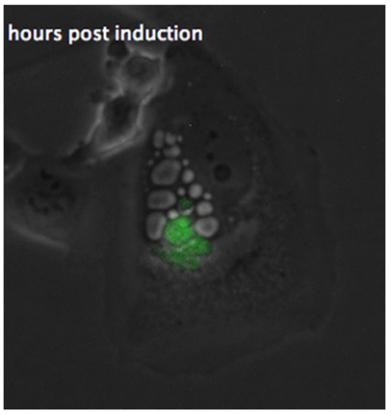

Movie S2. U2OS cells were challenged with the *Coxiella cvpB*::Tn complemented strain for 3 d in the absence of aTc. Complementation induction was triggered at the moment of image acquisition. Images were acquired every 10 min for 32 h in the phase-contrast and GFP channels.

Movie S2

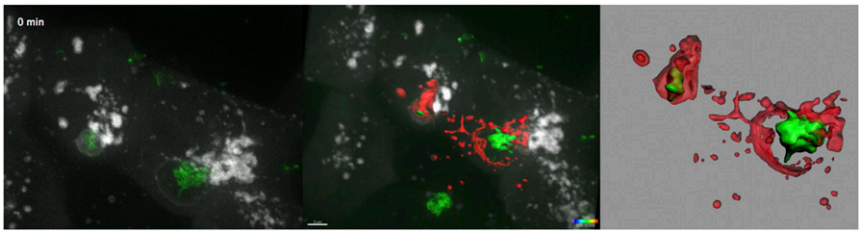

Movie S3. U2OS cells expressing mCherry-2xFYVE were challenged with the *Coxiella* control transposon mutant *Tn1832* for 3 d before imaging using a spinning-disk confocal microscope. Image stacks were acquired every 2 min in the mCherry (white) and GFP channels (green) for 3 h (*Left*). Surface rendering of mCherry-2xFYVE–positive compartments and *Coxiella* colonies was performed with IMARIS software on two ROIs. Surface rendering was superimposed to the image sequence (*Middle*) or extracted for easier visualization (*Right*).

Movie S3

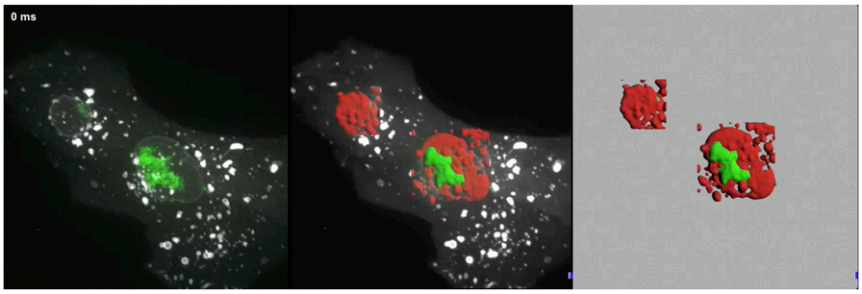

Movie S4. U2OS cells expressing mCherry-2xFYVE were challenged with the *Coxiella* complemented mutant *cvpB*::Tn Comp. for 3 d before imaging by using a spinning-disk confocal microscope. Image stacks were acquired every 2 min in the mCherry (white) and GFP channels (green) for 40 min (*Left*). Surface rendering of mCherry-2xFYVE–positive compartments and *Coxiella* colonies was performed with IMARIS software on two ROIs. Surface rendering was superimposed to the image sequence (*Middle*) or extracted for easier visualization (*Right*).

Movie S4

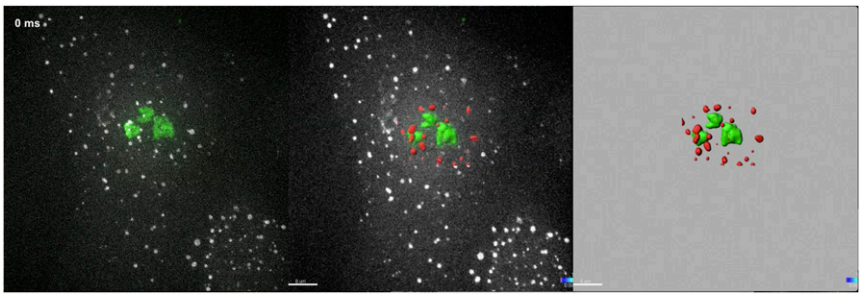

Movie S5. U2OS cells expressing mCherry-2xFYVE were challenged with the *Coxiella* mutant *cvpB*::Tn for 3 d before imaging by using a spinning-disk confocal microscope. Image stacks were acquired every 2 min in the mCherry (white) and GFP channels (green) for 40 min (*Left*). Surface rendering of mCherry-2xFYVE–positive compartments and *Coxiella* colonies was performed with IMARIS software on two ROIs. Surface rendering was superimposed to the image sequence (*Middle*) or extracted for easier visualization (*Right*).

Movie S5

Other Supporting Information Files

SI Appendix (PDF)

SUPPORTING INFORMATION

Supporting Methods

Antibodies and reagents

Generation of anti-*C. burnetii* NMII antibodies in rabbits was performed by Covalab. Hoechst 33258, anti-mouse and anti-rabbit HRP-conjugated antibodies, Atto-647N phalloidin, rabbit anti-GST and anti-His HRP-conjugated antibodies, polyclonal anti-LAMP1, polyclonal anti-ATG7, monoclonal anti-HA and polyclonal anti-LC3 antibodies were purchased from Sigma. Polyclonal anti-HA antibody was from Santa Cruz. Monoclonal anti-β Lactamase (BLAM) antibody was from Pierce. Polyclonal anti-EEA1 antibody was from EMD Millipore. Polyclonal anti-ATG5 and monoclonal anti-Rab5 and anti-Rab7 antibodies were from Cell Signaling. Monoclonal anti-LC3 antibody was from Enzo Life Sciences. Monoclonal anti-PIKfyve was from AbD Serotec. Monoclonal anti-GAPDH was from Life Technologies. Monoclonal anti-GM130 was purchased from BD Biosciences. Mouse and rabbit IgG conjugated to Alexa Fluor 488, 555 or 647 as well as Prolong Gold antifade mounting reagent were purchased from Invitrogen. Gold-labelled goat anti-rabbit antibody was purchased from British Biocell International. Paraformaldehyde, glutaraldehyde, osmic acid, epon 812, propylene oxide, 300 mesh nickel grids, formvar/carbon-coated nickel grids, formaldehyde and Lowicryl K4M were purchased from Electron Microscopy Sciences. LY294002 was purchased from Gibco. YM201636 was from Santa Cruz. Spautin-1 and 3-Methyladenine (3-MA) were purchased from Sigma. FITC-labelled Cholera toxin B was purchased from Life Technologies. Active, GST-tagged human Vps34 was purchased from Sigma. siRNA oligonucleotides were purchased from Dharmacon. Purified Egg PC, brain PS and 18:1 PI(3)P were from Avanti Polar Lipids, Inc.

Plasmids

Plasmids and primers used in this study are listed in Table 2 and 3, respectively. DNA sequences were amplified by PCR using Phusion polymerase (New England Biolabs) and gene-specific primers (Sigma).

Plasmid design for mammalian cells transfection

In order to generate the plasmid pLVX-mCherry-N2, pLVX-mCherry-C1 was amplified by inverse PCR using primers PLVX-MluI-NotI-Fw and PLVX-MluI-Rv. Following digestion with MluI, the vector was ligated to obtain circular pLVX-mCherry-N2. pUC57-Kan containing the eukaryotic codon-optimised sequence of CvpB (CvpBopt) was obtained from Genscript. CvpBopt was amplified from pUC57-Kan-CvpBopt using primers pairs CvpBopt-AgeI-Fw/CvpBopt-BamHI-Rv and CvpBopt-MluI/CvpBopt-NotI, and the PCR products were cloned into pcDNA3.1-BirA-HA and pLVX-mCherry-N2, respectively. For cloning of N-terminal truncations of CvpBopt in pLVX-mCherry-N2, CvpBopt was amplified using forward primers CvpBopt100-809-MluI-Fw, CvpBopt200-809-MluI-Fw, CvpBopt400-809-MluI-Fw, CvpBopt500-809-MluI-Fw or CvpBopt600- 809-MluI-Fw and reverse primer CvpBopt-NotI-Rv. For cloning of C-terminal truncation of CvpBopt in pLVX-mCherry-N2, CvpBopt was amplified using forward primers CvpBopt-MluI-Fw and reverse primers CvpBopt1-200-NotI-Rv, CvpBopt1-400-NotI-Rv, CvpBopt1-500-NotI-Rv, or CvpBopt1-600-NotI-Rv. In order to generate pLVX-mCherry-C1-Rab5, Rab5 was amplified from pCI-Rab5 using primers Rab5-EcoRI-Fw/Rab5-BamHI-Rv and cloned into pLVX-mCherry-C1._In order to generate pCI-Neo-mCherry-2xFYVE, mCherry-2xFYVE was amplified from pL17mCFywt using the primer pair Cherry-NheI-Fw/PL17-EcoRI-Rv and cloned into pCI-Neo.

Plasmid design for protein expression in Escherichia coli

CvpB was amplified from *Coxiella* RSA439 NMII genomic DNA using primers CvpB-EcoRI-Fw and CvpB-SalI-Rv and cloned into pGEX4T1 to obtain pGEX4T1-CvpB. To generate His-tagged CvpB, 1-500 and 500-809 domains of CvpB, the corresponding DNA sequences were amplified from *Coxiella* RSA439 NMII genomic DNA using primer pairs CvpB-EcoRI-Fw/CvpB-SalI-Rv, CvpB-EcoRI-Fw/CvpB1-500-SalI-Rv and CvpB500-809-EcoRI-Fw/CvpB-SalI-Rv and cloned into pET28a to generate pET28a-CvpB, pET28a-$CvpB_{1\text{-}500}$ and pET28a-$CvpB_{500\text{-}809}$, respectively.

Plasmid design for secretion assay in C. burnetii

CvpB, CvpBdE and CBU_2052 were amplified from *Coxiella* RSA439 NMII genomic DNA using primer pairs CvpB-SalI-Fw/CvpB-SphI-Rv, CvpB-SalI-Fw/ CvpBdE-SphI-Rv and 2052-SalI-Fw/2052-SphI-Rv, respectively. PCR products were cloned into pJB-CAT-Blam to generate pJB-CAT-Blam-CvpB, pJB-CAT-Blam-CvpBdE and pJB-CAT-Blam-CBU_2052, respectively.

Plasmid design for CvpB complementation in C. burnetii

TetRA was amplified from pJB-CAT-TetRA using the primer pair TetR-NheI-Fw/TetR-PstI-Rv and cloned into pUCR6K-miniTn7-Kan to generate pUCR6K-miniTn7-Kan-TetRA. *cvpB* was amplified from *Coxiella* RSA439 NMII genomic DNA using primers CvpB-XmaI-Fw/CvpB-EcoRI-Rv and cloned into pRK5-HA to obtain pRK5-HA-CvpB. HA-CvpB was amplified from pRK5-HA-CvpB using primers HA-PstI-Fw/CvpB-EcoRI-Rv and cloned into pUCR6K-miniTn7-Kan-TetRA to generate pUCR6K-miniTn7-Kan-TetRA-HA-CvpB. The 4xHA tag was amplified from pMMB207C-HAx4 using primers 4xHA-PstI-Fw/4xHA-EcoRI-Rv and cloned into pUCR6K-miniTn7-Kan-TetRA to generate pUCR6K-miniTn7-Kan-TetRA-4xHA. CvpB was amplified from *Coxiella* RSA439 NMII genomic DNA using primers CvpB-XmaI-Fw/CvpB-EcoRI-Rv

and cloned into pUCR6K-miniTn7-Kan-TetRA-4xHA to obtain pUCR6K-miniTn7-Kan-TetRA-4xHA-CvpB.

Image-based supervised machine learning

The identification of transposon insertion leading to multivacuolar phenotypes was performed using the Classifier package of the CellProfiler Analyst software. Random images acquired from cells infected either with *Coxiella* Tn1832 or with the *icmS*::Tn mutant were manually sorted into two classification bins (single vacuole and multivacuolar phenotypes, respectively) to form a training set that is used by Classifier to generate rules for differentiating among objects in each bin. Classifier then scored our image database, which included classifying all objects in each image, count how many object in each class are represented in each image and computing the enrichment/depletion of each class per image. Enrichment scores are computed for each sample as the logit area under the ROC curve for the prior versus the posterior distribution. The prior is computed from the full experiment using a Dirichlet-Multinomial distribution fit to the groups, and the posterior is computed for each group independently; that is, each phenotype is treated as positive and all others as negative for each phenotype in turn.

Beta-Lactamase translocation assay

For *C. burnetii* effector translocation assays, cells were cultured in black, clear-bottomed, 96-well plates and infected with the appropriate *C. burnetii* strain (MOI of 100) for 24 and 48 h. *C. burnetii* expressing Beta-Lactamase alone were used as negative control; *C. burnetii* expressing Beta-Lactamase-tagged CBU_2052 was used as positive control. Cell monolayers were loaded with the fluorescent substrate CCF4/AM (LiveBLAzer-FRET B/G loading kit; Invitrogen) in a solution containing 20 mM HEPES, 15 mM probenecid (Sigma) pH 7.3, in HBSS. Cells were incubated in the dark for 1 h at room temperature and imaged using an EVOS inverted

fluorescence microscope. Images were acquired using DAPI and GFP filter cubes. The image analysis software CellProfiler was used to segment and identify all cells in the sample (GFP) and positive cells (DAPI) and to calculate the intensity of fluorescence in each channel. The percentage of positive cells versus the total number of cells was then calculated and used to evaluate effector translocation.

Intracellular replication of *Coxiella*

Cells were seeded into 96-wells plates (Greiner Bio one) 2 days prior to infection. Cells were then challenged with *C. burnetii* strains at an MOI of 100. Bacterial contact with cells was promoted by centrifugation (10 min, 400 x g, RT) and cells were incubated in a humidified atmosphere of 5% CO_2 at 37°C. Unbound bacteria were removed after 1h of incubation and cells were further incubated in fresh culture medium for 7 days. Plates were analyzed at a 24-hours interval using a TECAN Infinite 200 Pro operated by the Magellan software (TECAN) to monitor the variations of GFP fluorescence associated with the intracellular growth of *Coxiella*.

Transmission electron microscopy

For morphology-EM, cells were fixed in 2.5% glutaraldehyde in 0.1M phosphate buffer for 1 hour at 4°C, post fixed in 1% osmic acid 1 hour at 4 °C and 0.5% tannic acid 30min at 4 °C. Cells were then dehydrated and infiltrated with mixes of epon 812/propylene oxide with increasing concentrations of epon before embedding. Ultrathin sections were cut with a Reichert Ultracut (Leica) ultramicrotome and collected with 300 mesh nickel grids, stained with 0.2% oolong tea extract 30 min (OTE, Delta microscopies) and lead citrate 4 min. For immuno-EM, cells were fixed in 4% formaldehyde and 0.05% glutaraldehyde in 0.1M phosphate buffer for 1 hour at 4 °C, quenched with 0.05M NH_4Cl in 0.1M phosphate buffer for 30 minutes. After dehydration, cells were infiltrated with mixes of resin (Lowicryl K4M) and ethanol with increasing concentrations of resin and then embedded. Ultrathin sections were cut

with a Reichert Ultracut (Leica) ultramicrotome and collected with 300 mesh, formvar/carbon-coated nickel grids. After blocking 20 minutes in Tris buffer (TB; 20 mM Tris-HCl pH 8.2, 1% BSA, 1% goat serum), immunogold labelling was performed by incubating sections overnight at 4 °C with a rabbit anti-HA antibody diluted 1/50 in TBS and one hour at room temperature with 20 nm gold labelled goat anti-rabbit diluted 1/20 in TBS supplemented with 1% teleostean gelatine (Sigma). Finally, the grids were stained 20 minutes with 2% uranyl acetate. Observations were made on a Tecnai G2 F20 (200KV , FEG) electron microscope.

Live imaging

To monitor the formation of *C. burnetii* parasitophorous vacuoles, U2OS cells cultured in 6-well plates were challenged with either *C. burnetii Tn1832*, *cvpB*::Tn or the corresponding complemented strain (*cvpB*::Tn Complemented) at an MOI of 100. Gene complementation was induced either at the moment of infection or four days post-infection by adding 400 ng/ml anhydrotetracycline (aTc, Santa Cruz) to the culture medium. Three days post-infection cells were imaged using an Olympus IX83 inverted microscope equipped with an ANDOR Zyla 4.2 sCMOS camera, a 10X ph objective in a temperature- and CO_2-controlled chamber. Images were acquired every 10 min over 48 hours. To monitor the dynamics of PI(3)P at the *C. burnetii* parasitophorous vacuole, U2OS cells expressing mCherry-2xFYVE cultured in glass-bottomed 35 mm dishes were challenged with *C. burnetii*, *cvpB*::Tn or *cvpB*::Tn Complemented, at an MOI of 100. Three days post-infection cells were imaged using an inverted Nikon Ti Eclipse microscope equipped with an ANDOR confocal spinning disk, an emCCD iXion Ultra camera in a temperature- and CO_2-controlled chamber. Image stacks were acquired every 2 min using a 100X oil immersion objective. In all cases, ICY software was used for image analysis. 3D reconstruction and surface rendering were performed using IMARIS.

Protein expression and purification

Genes cloned into pGEX-4T1 or pET28a vectors were expressed in *Escherichia coli* XL1-blue or BL21(DE3) star, respectively. Bacterial cultures were grown at 37°C to mid-exponential phase (OD_{600nm}=0.5) and induced for 4 h with 0.5 mM IPTG. Bacteria were harvested by centrifugation, resuspended in GST lysis buffer (20 mM Tris-HCl pH 8, 300 mM NaCl, 5 % glycerol, complete anti-protease (Roche)) or His lysis buffer (20 mM Tris-HCl pH 8, 300 mM NaCl, 5 mM imidazole, complete anti-protease (Roche)) and lysed with Bugbuster (Novagen) following the manufacturer's recommendations. Lysates were cleared by centrifugation (11 000 g, 20 min, 4°C). Proteins were purified by gravity flow using glutathione-sepharose (Sigma) for GST-tagged proteins, or HIS Select Nickel affinity resin (Sigma) for histidine-tagged proteins. GST- and Histidine-tagged proteins were eluted with lysis buffer supplemented with 25 mM reduced glutathione or 250 mM imidazole, respectively.

Cell fractionation

U2OS cells grown to 60% confluence in three T75 flasks were infected with *C. burnetii Tn1832*, *cvpB*::Tn or *cvpB*::Tn Complemented at an MOI of 100, uninfected cells were used as negative control. After 3 days of infection, cells were washed with PBS and detached from the flasks using trypsin-EDTA 0.25% and pelleted for 5 min at 200 x g. Pellets were resuspended in 4 ml of HS buffer (20 mM HEPES pH 7.2, 0.25 M sucrose, 1 mM EDTA and protease inhibitors (Complete, Roche)) and lysed using a stainless-steel ball homogenizer (9 strokes, 16-µm clearance, Isobiotec). Homogenates were visually analysed for presence of CCVs using fluorescence and light microscopy (Evos microscope, Life Technologies). Homogenates were then spun at 600 x g for 15 min at 4°C and the supernatant (SN) was kept for Western blot analysis. The pellet was resuspended in 500 µl of HS buffer before being loaded onto a 12 ml cushion of a 10-35% linear gradient of Histodenz (Sigma) in PBS (15 ml

195 Falcon tubes). Samples were centrifuged (1 h, 3400 x g, 4°C), separated into 8
196 fractions of 1.5 ml and analysed by Western blot.
197
198 *Galleria mellonella* survival assay
199 Larvae were purchased from Live Foods UK and maintained on wood chips at 14 °C.
200 Groups of 30 larvae weighing 0.25–0.35 g were injected with 10^6 GE ml $^{-1}$ *C. burnetii*
201 NMII, *Tn1832* or *cvpB*::Tn into the uppermost right proleg. The larvae were incubated
202 at 37 °C and survival was monitored at 24 h intervals. Larvae were scored as dead
203 when they displayed no movement in response to gentle manipulation with a pipette
204 tip. PBS-injected controls were included and each experiment was carried out in
205 triplicate. To determine bacterial numbers, at 96 h and 120 h post-infection, three
206 larvae were placed on ice for 10 min to prevent movement. The bottom 2 mm of each
207 larva was aseptically removed and haemolymph was drained into a sterile
208 microcentrifuge tube. Bacterial burden was determined using real-time PCR. *C.*
209 *burnetii* was enumerated using real-time PCR targeting the *com1* gene. The Com1
210 probe was covalently labelled at the 5' end with the reporter dye FAM and at the 3'
211 end with the quencher dye BHQ-1. Primers and probe were purchased (ATDBio).
212 Chromosomal DNA was extracted by addition of 100 µl sample to 900 µl Instagene
213 Matrix (Bio-Rad). The Instagene/sample suspension was heated (95 °C ; 15 min),
214 centrifuged (10000 r.p.m.; 3 min; Eppendorf Microcentifuge model no. 5424) and
215 supernatant was retained for PCR. PCR cycling conditions comprised 3 min at 95 °C,
216 30 s at 60 °C, followed by 50 two-step cycles of 15 s at 95 °C and 30 s at 60 °C.
217

Supporting Figure 1

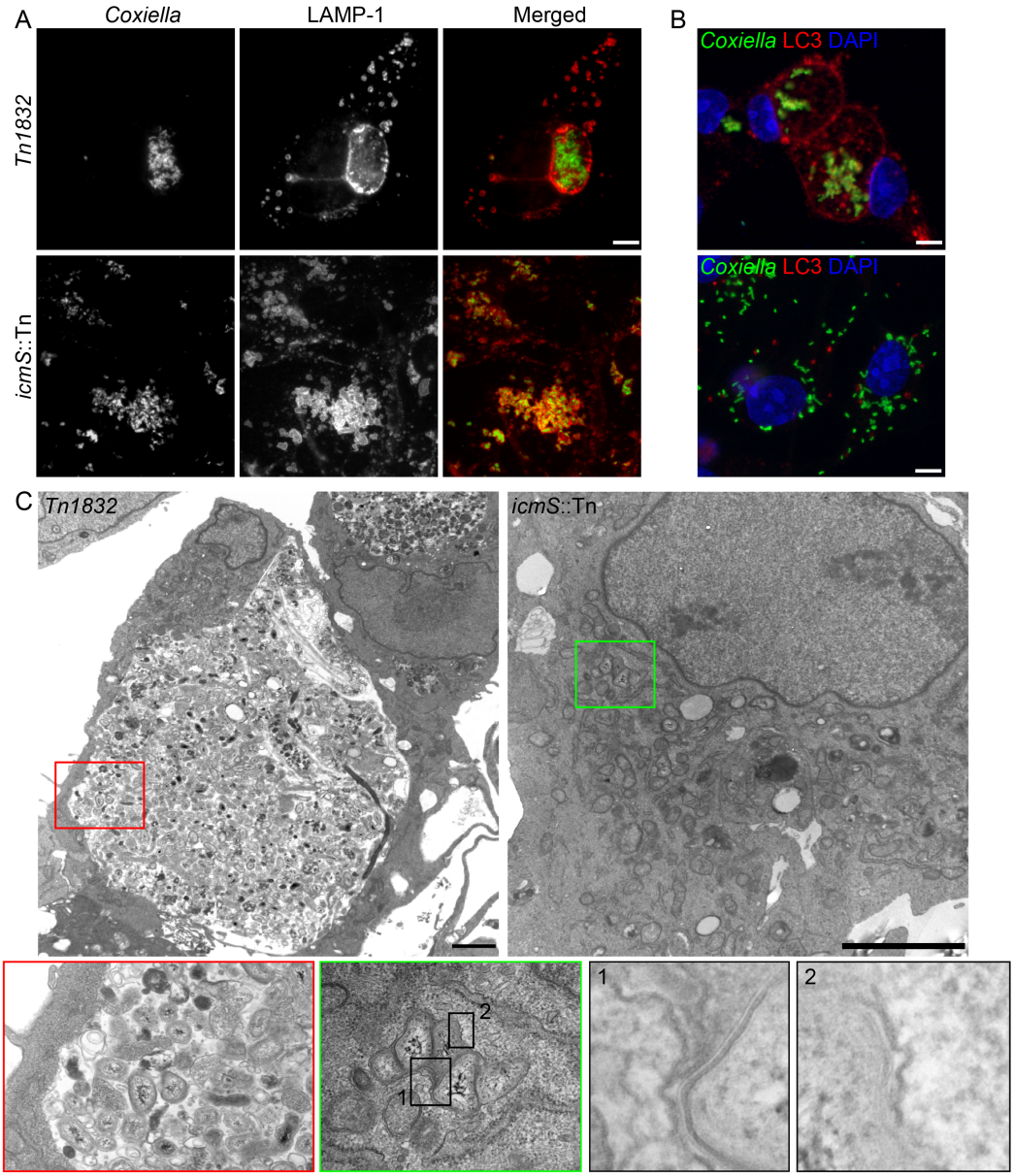

228 **Supporting Figure 2**

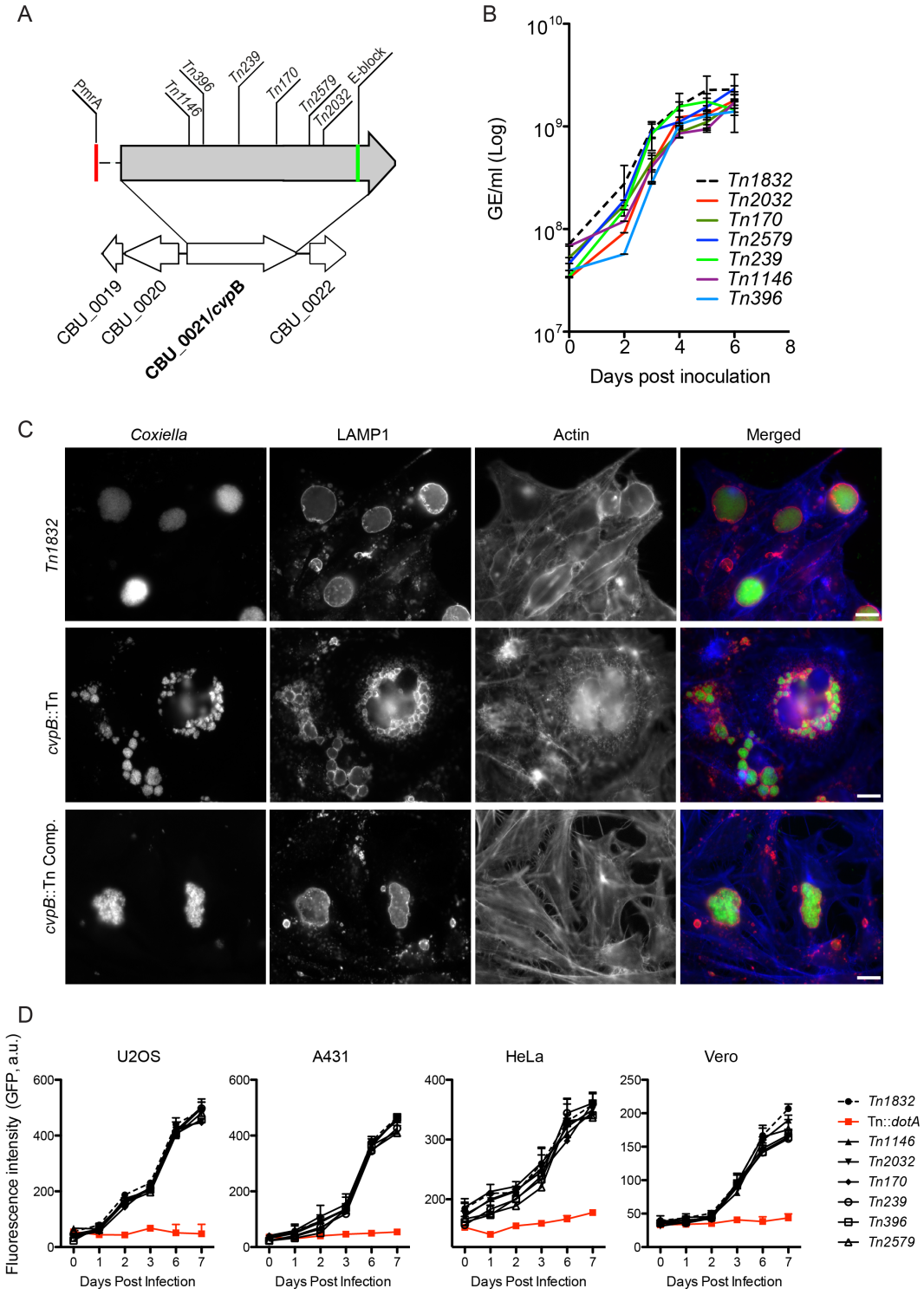

229

230

231

232

Supporting Figure 3

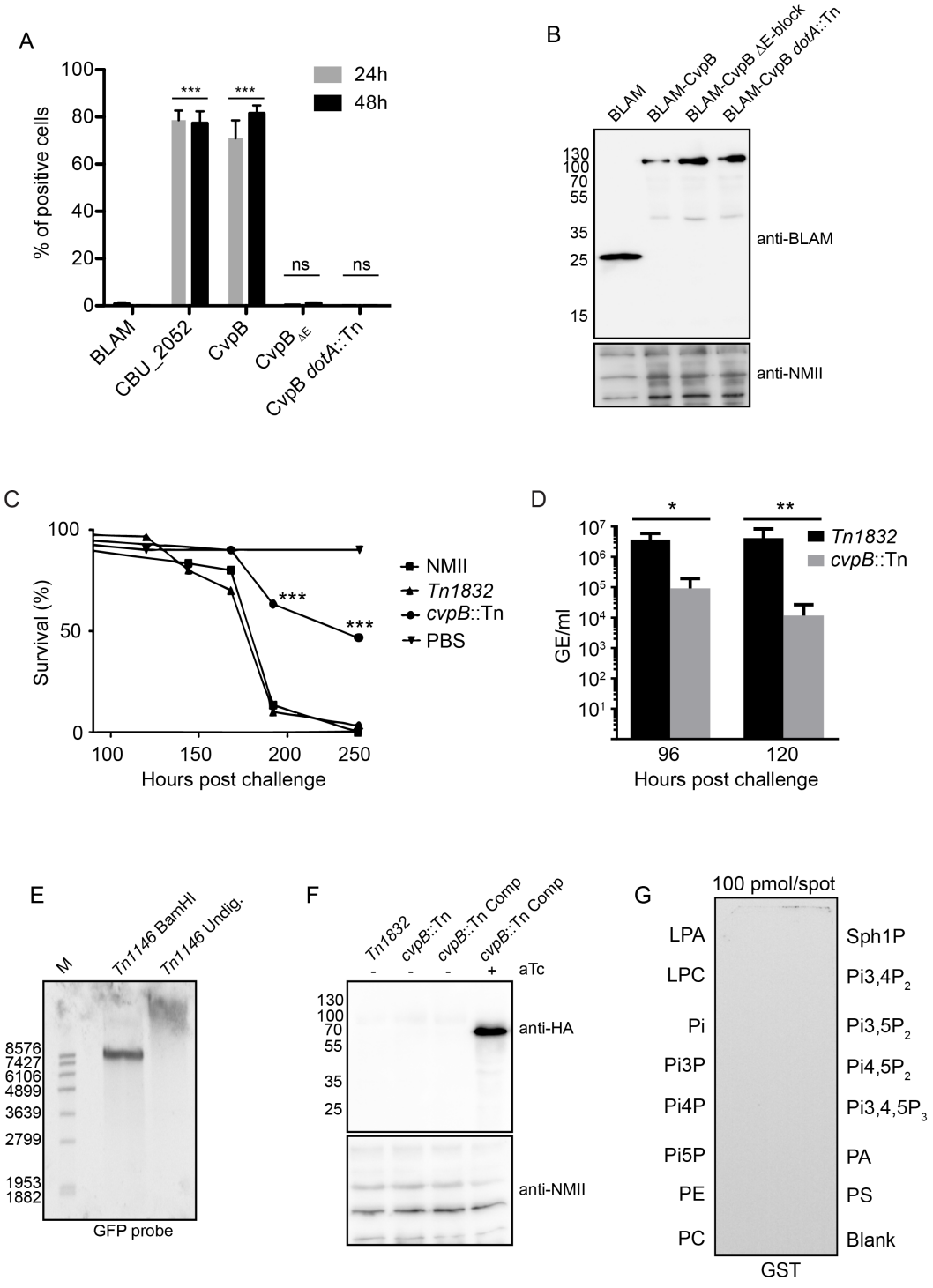

Supporting Figure 4

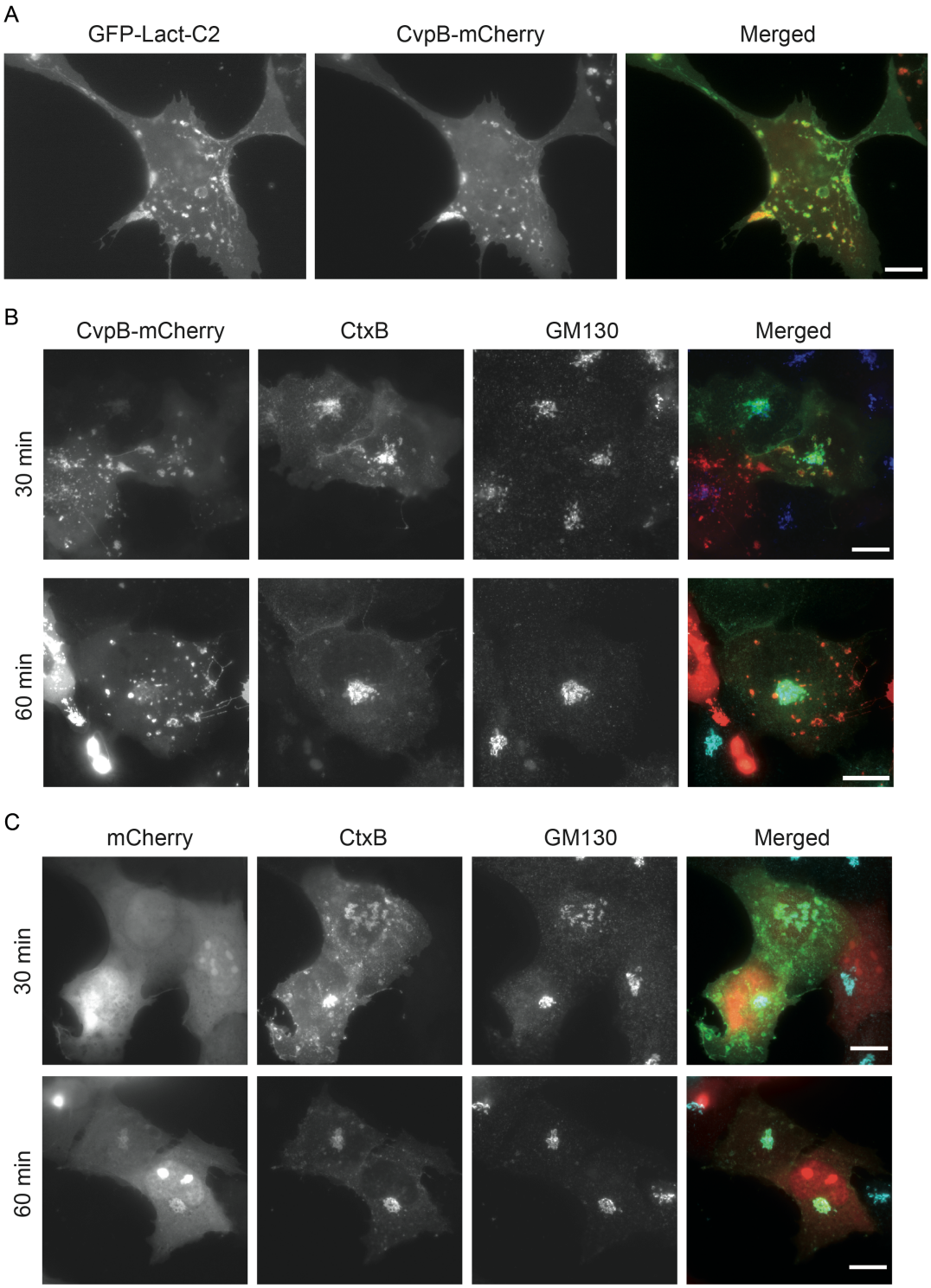

Supporting Figure 5

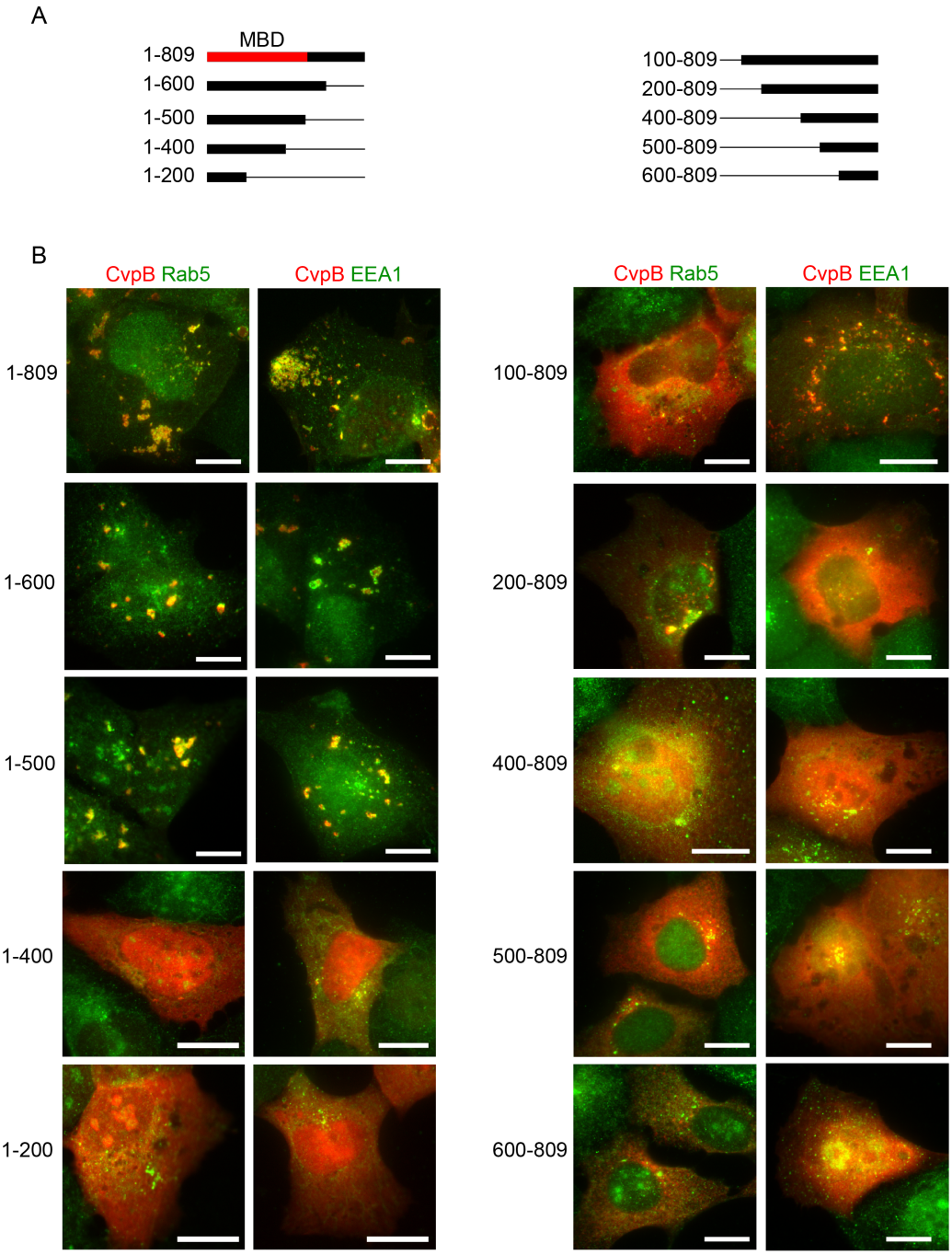

Supporting Figure 6

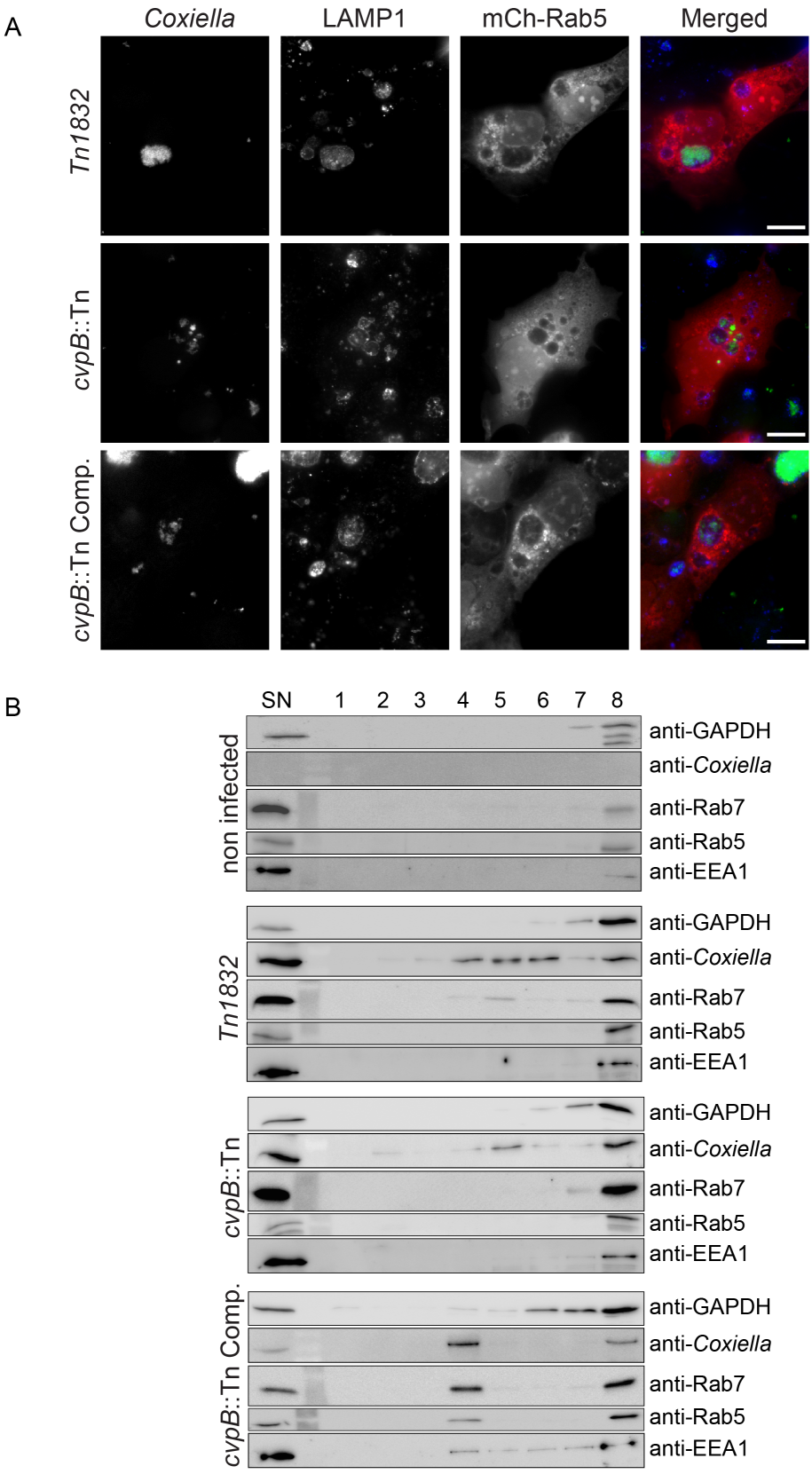

Supporting Figure 7

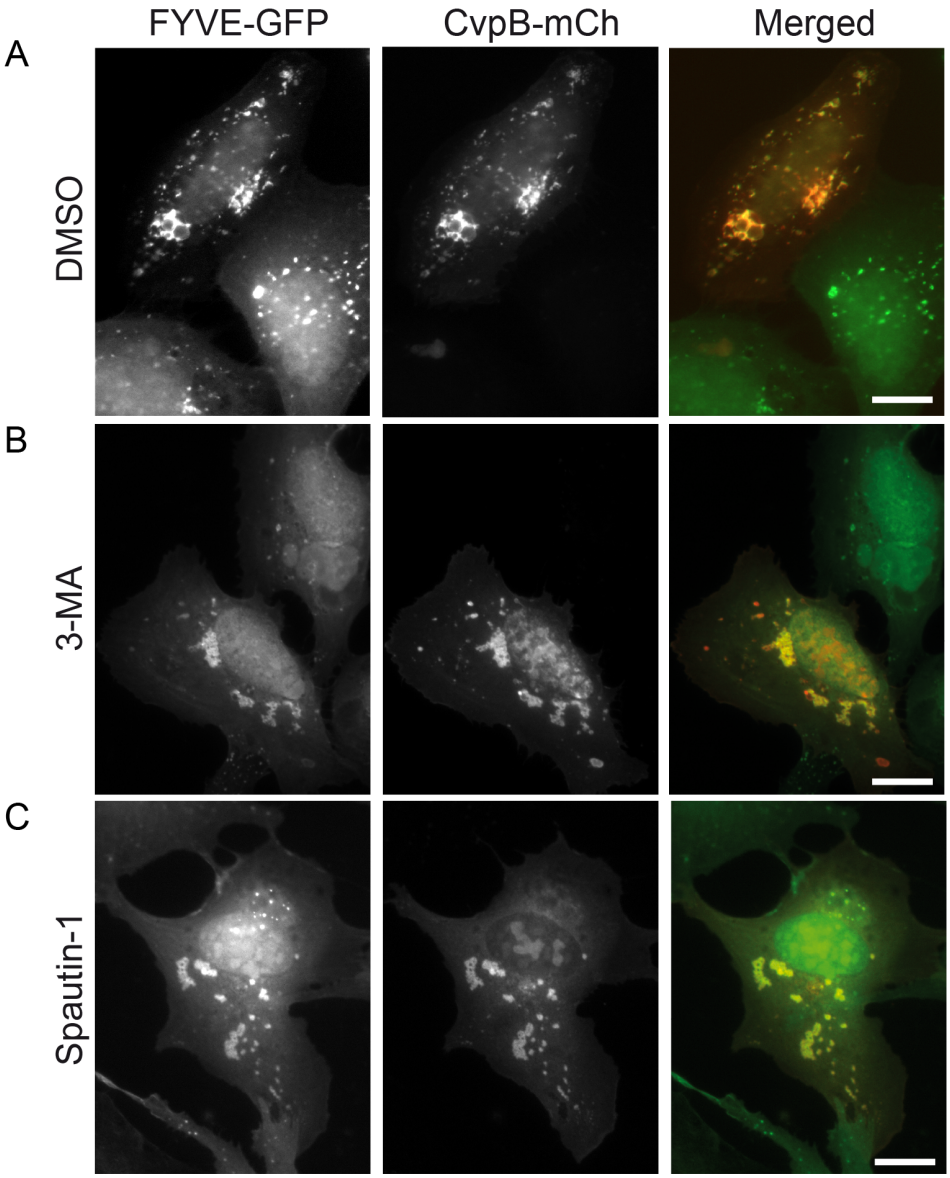

Supporting Figure 8

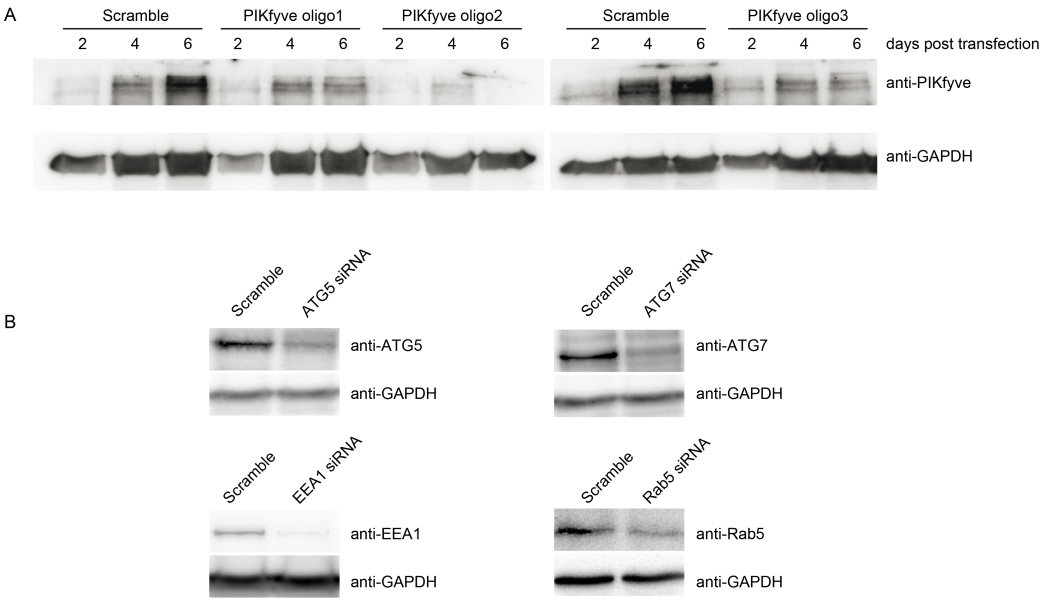

Supporting Figure Legends

Supporting Figure 1. Transposon insertion in *Coxiella* chaperone-encoding gene *icmS* leads to a multi-vacuolar phenotype. Vero cells were infected with the control transposon mutant *Tn1832* (top panels) or the *icmS*::Tn mutant (bottom panels) and fixed after 5 days of infection. *Coxiella* colonies were visualised using transposon-encoded GFP (green); antibodies against LAMP1 (A) or LC3 (B) coupled to Alexa Fluor 555 (red) were used to visualise CCVs and autophagosomes, respectively. Scale bars = 5 µm. (C) Cells infected as above were processed for transmission electron microscopy. Red box and inset indicate the presence of a large number of bacteria and cellular material inside *Tn1832*-generated vacuoles. Green box and inset indicate that *icmS*::Tn-generated vacuoles are tight-fitting and contain less bacteria and no cellular material (Insets 1 and 2: details of the vacuolar membrane). Scale bars = 2 µm.

Supporting Figure 2. CvpB is a Dot/Icm secreted effector required for optimal CCV biogenesis and virulence. (A) Schematic representation of the genomic context of CBU_0021 and sites of transposon insertion of 6 independent isolated mutants (*Tn1146*, *Tn396*, *Tn239*, *Tn170*, *Tn2579* and *Tn2032*). The regulatory element PmrA is represented in red and the predicted E-block motif is indicated in green. (B) Axenic (ACCM-2) growth of 6 independent *cvpB*::Tn mutants. Control transposon mutant *Tn1832* (dashed black line) was used as control. Values are mean ± SD of triplicate experiments. (C) HeLa cells were infected with either *Coxiella Tn1832* (top panels), *cvpB* ::Tn (middle panels) or the complemented *cvpB* ::Tn strain (*cvpB*::Tn Comp., bottom panels). Six days post-infection, cells were fixed and stained with anti-LAMP1 (red) and phalloidin (blue). Scale bars = 10 µm. (D) U2OS, A431, HeLa and Vero cells were challenged either with each cvpB transposon mutants isolated, with the control *Coxiella* mutant *Tn1832* or with the *dotA*::Tn

mutant. Intracellular replication of *Coxiella* was assessed by monitoring the GFP expressed by the mutants using a microplate reader. Values are mean ± SD from 3 independent experiments.

Supporting Figure 3. (A) HeLa cells were infected for 24h or 48h with *Coxiella* NMII or the *dotA*::Tn mutant transformed with vectors expressing Beta-Lactamase alone (BLAM, negative control), BLAM-CBU_2052 (positive control), BLAM-CvpB or BLAM-$CvpB_{\Delta E\text{-block}}$ ($CvpB_{\Delta E}$). Secretion of these proteins was probed using the CCF-4 substrate. The average percentage of cells positive for cleaved CCF-4 as compared to the total number of cells was assessed. Values are mean ± SD from 3 independent experiments. ns = non-significant; *** = P<0.0001 (1-way ANOVA).(B) Expression of Beta-lactamase (BLAM)-CvpB fusion proteins used for experiments in Fig. S3A. Bacterial extracts were analysed by Western blot using anti-BLAM (top panel) and anti-*Coxiella* NMII (bottom panel) antibodies. (C) Survival chart of *Galleria mellonella* larvae infected with either *Coxiella* NMII (squares), the control mutant *Tn1832* (triangles) or the *cvpB* ::Tn mutant (circles). PBS-injected larvae were used as control (inverted triangles). Values are means of three replicates, each with 30 injected larvae per condition. *** = P<0.0001 (*cvpB*::Tn vs. NMII or Tn1832, Long Rank Mantel-Cox analysis). (D) Real-time PCR targeting the *Coxiella* gene *com1* was carried out on *Galleria mellonella* larvae infected with the *Coxiella* control transposon mutant *Tn1832* or the *cvpB*::Tn mutant at the indicated time points. * = P<0.05, ** = P<0.01 (2-way ANOVA, Bonferroni's multiple comparison test). (E) *cvpB*::Tn mutant *Tn1146* genomic DNA was either digested with the restriction enzyme BamHI (*Tn1146* BamHI) or left undigested (*Tn1146* Undig.) prior to migration on agarose gel and Southern blot analysis using a fluorescent GFP probe. The band observed at 8155 bp confirms the unique insertion of the transposon in *cvpB*. (F) Expression of HA-tagged CvpB in *cvpB*::Tn complemented strain in the presence or absence of 400 ng/ml anhydrotetracycline (aTc). Bacterial extracts were

318 analysed by Western blot using anti-HA and anti-*Coxiella* NMII antibodies. (G)
319 Protein-lipid overlay assay performed with GST alone showed no lipid binding
320 activity.
321
322 **Supporting Figure 4.** (A) U2OS cells were co-transfected with pGFP-Lact-C2
323 (green) and pLVX-CvpB-mCherry (red). CvpB and the PS probe Lact-C2 colocalise
324 in transfected cells. U2OS cells were transfected either with pLVX-CvpB-mCherry (B)
325 or pLVX-mCherry (C) and incubated with FITC-labelled Cholera toxin B (CtxB) for 60
326 min on ice. Cells were then incubated at 37 °C for 30 or 60 min, fixed and labelled
327 with anti-GM130 coupled to Alexa Fluor 647 (blue). Scale bars = 10 µm.
328
329 **Supporting Figure 5. (**A) Schematic representation of the CvpB fragments
330 ectopically-expressed as mCherry fusion proteins (MBD = Membrane-Binding
331 Domain). (B) U2OS cells were transiently transfected with pLVX-CvpB-mCherry (1-
332 809) or CvpB fragments cloned into pLVX-mCherry (red), fixed and labelled with anti-
333 Rab5 or anti-EEA1 antibodies (green). Systematic analysis of colocalisation between
334 the CvpB fragments and Rab5- or EEA1-positive vesicles reveals that CvpB has a
335 MBD spanning from amino acids 1-500, that is necessary for membrane targeting.
336 Scale bars = 10 µm.
337
338 **Supporting Figure 6.** (A) U2OS cells were transfected with mCherry-Rab5 and
339 challenged with either *Coxiella Tn1832*, the *cvpB*::Tn mutant or the complemented
340 strain for 3 days. *Coxiella* colonies, Rab5-positive vesicles and LAMP1 were
341 detected using GFP (green), mCherry (red) and an anti-LAMP1 antibody coupled to
342 Alexa Fluor 647 (blue), respectively. Scale bars = 10 µm. (B) U2OS cells uninfected
343 or infected for 3 days with either *Coxiella Tn1832*, the *cvpB*::Tn mutant or the
344 complemented strain were lysed and separated into pellet and supernatant (SN) by
345 low speed centrifugation. The pellet was further separated onto a linear gradient of

Histodenz and the fractions 1 (bottom of the gradient) to 8 (top of the gradient) were analysed by Western blot using antibodies against GAPDH, *Coxiella*, Rab7, Rab5 and EEA1. Lack of GAPDH was used as a proxy for efficient cell lysis and the concomitant presence of *Coxiella* and Rab7 in fractions was used to identify fractions enriched in CCVs.

Supporting Figure 7. U2OS GFP-2xFYVE (green) cells were incubated either with DMSO (A), the PI 3-kinase inhibitors 3-MA (B) or Spautin-1 (C) for 4 h and transfected with pLVX-CvpB-mCherry (red) for 12 h (See also corresponding Fig. 5B). Scale bars = 10 µm.

Supporting Figure 8. (A) U2OS cells were transfected for 2, 4 and 6 days with either Scramble or PIKfyve-targeting (oligo1, oligo2 or oligo3) siRNA. PIKfyve expression level was detected by Western blot using an anti-PIKfyve antibody. Anti-GAPDH was used as loading control. All PIKfyve-targeting siRNAs decreased the expression levels of PIKfyve, oligo2 being the most efficient. (B) U2OS cells were transfected for 5 days with the indicated siRNAs. Protein expression levels were detected by Western blot using specific antibodies. Anti-GAPDH was used as loading control.

366 **Table 1. List of strains used in this study**

Strain	Description	Origin
wt Coxiella burnetii	*Coxiella burnetii RSA 439 Nine Mile II*	Robert Heinzen
Coxiella Tn1832	*Coxiella burnetii* RSA 439 Nine Mile II carrying a transposon GFP-CAT between CBU_1847b and CBU_1849	(1)
Coxiella Tn1146	Coxiella burnetii RSA 439 Nine Mile II carrying a transposon GFP-CAT in CBU_0021 (*cvpB*)	(1)
*Coxiella Tn1146*comp	Coxiella burnetii RSA 439 Nine Mile II carrying a transposon GFP-CAT in CBU_0021 (*cvpB*) and a transposon TetRA-HA-*cvpB*	This study
Coxiella Tn1146 4xHA-*cvpB*	Coxiella burnetii RSA 439 Nine Mile II carrying a transposon GFP-CAT in CBU_0021 (*cvpB*) and a transposon TetRA-4xHA-*cvpB*	This study
Coxiella Tn2098	Coxiella burnetii RSA 439 Nine Mile II carrying a transposon GFP-CAT in CBU_1642 (*icmS*)	(1)
Coxiella Tn292	Coxiella burnetii RSA 439 Nine Mile II carrying a transposon GFP-CAT in CBU_1648 (*dotA*)	(1)
XL-1 Blue	*E. coli* strain used for Ptac-driven recombinant protein expression	Clontech
BL21(DE3) star	*E. coli* strain used for T7-driven recombinant protein expression	Invitrogen

367

368

Table 2. List of plasmids used in this study

Name	Description	Origin
pLVX-mCherry-C1	CMV expression vector for N-terminal fusion of mCherry	Clontech
pCI-Rab5	Encodes human Rab5	Bruno Beaumelle
pLVX-mCherry-C1-Rab5	CMV expression vector expressing Rab5 with N-terminal fusion of mCherry tag	This study
pLVX-mCherry-N2	CMV expression vector for C-terminal fusion of mCherry	This study
pUC57-Kan-CvpBopt	Encodes codon-optimized sequence fo *cvpB* for eukaryotic expression (CvpBopt)	Genscript
pcDNA3.1-BirA-HA	CMV expression vector for C-terminal fusion of BirA-HA tag	Addgene
pcDNA3.1-CvpBopt-BirA-HA	CMV expression vector expressing CvpBopt with C-terminal fusion of BirA-HA tag	This study
pLVX-CvpBopt-mCherry-N2	CMV expression vector expressing CvpBopt with C-terminal fusion of mCherry tag	This study
pLVX-CvpBopt1-200-mCherry-N2	CMV expression vector expressing $CvpBopt_{1-200}$ with C-terminal fusion of mCherry tag	This study
pLVX-CvpBopt1-400-mCherry-N2	CMV expression vector expressing $CvpBopt_{1-400}$ with C-terminal fusion of mCherry tag	This study
pLVX-CvpBopt1-500-mCherry-N2	CMV expression vector expressing $CvpBopt_{1-500}$ with C-terminal fusion of mCherry tag	This study
pLVX-CvpBopt1-600-mCherry-N2	CMV expression vector expressing $CvpBopt_{1-600}$ with C-terminal fusion of mCherry tag	This study
pLVX-CvpBopt100-809-mCherry-N2	CMV expression vector expressing $CvpBopt_{100-809}$ with C-terminal fusion of mCherry tag	This study
pLVX-CvpBopt200-809-mCherry-N2	CMV expression vector expressing $CvpBopt_{200-809}$ with C-terminal fusion of mCherry tag	This study
pLVX-CvpBopt400-809-mCherry-N2	CMV expression vector expressing $CvpBopt_{400-809}$ with C-terminal fusion of mCherry tag	This study
pLVX-CvpBopt500-809-mCherry-N2	CMV expression vector expressing $CvpBopt_{500-809}$ with C-terminal fusion of mCherry tag	This study
pLVX-CvpBopt600-809-mCherry-N2	CMV expression vector expressing $CvpBopt_{600-809}$ with C-terminal fusion of mCherry tag	This study

pGEX-4T1	Ptac expression vector encoding glutathione S-transferase (GST)	GE Healthcare
pGEX-4T1-CvpB	Ptac expression vector encoding GST-CvpB	This study
pET28a	T7 expression vector	Novagen
pET28a-CvpB	T7 expression vector encoding His-CvpB	This study
pET28a-CvpB1-500	T7 expression vector encoding His-$CvpB_{1-500}$	This study
pET28a-CvpB500-809	T7 expression vector encoding His-$CvpB_{500-809}$	This study
peGFP-Lactadherin-C2	Encodes GFP-Lactadherin-C2	Addgene
pGFP-HA-PIKFYVE	Encodes GFP-PIKFYVE	Assia Shisheva
pCI-Neo	CMV expression vector	Promega
pL17mCFywt	Encodes mCherry-2xFYVE	Kai Wengelnik
pCI-Neo-mCherry-2xFYVE	Encodes mCherry-2xFYVE	This study
pGFP-LC3B	Encodes GFP-LC3B	Martine Biard
pGFP-LC3C	Encodes GFP-LC3C	Martine Biard
pJB-CAT-Blam	*Coxiella* P1169 expression vector for N-terminal fusion of Beta-lactamase enzyme	Robert Heinzen
pJB-CAT-Blam-CvpB	*Coxiella* P1169 expression vector expressing CvpB with N-terminal fusion of Beta-lactamase enzyme	This study
pJB-CAT-Blam-CvpBdE	*Coxiella* P1169 expression vector expressing $CvpB_{\Delta E\text{-}block}$ with N-terminal fusion of Beta-lactamase enzyme	This study
pJB-CAT-Blam-CBU_2052	*Coxiella* P1169 expression vector expressing CBU_2052 with N-terminal fusion of Beta-lactamase enzyme	This study
pRK5-HA	CMV expression vector for N-terminal fusion of HA tag	Gunnar Schroeder
pRK5-HA-CvpB	CMV expression vector expressing CvpB with N-terminal fusion of HA tag	This study
pJB-CAT-TetRA	*Coxiella* anhydrotetracycline-inducible expression vector	Robert Heinzen
pMMB207C-HAx4	*Legionella* expression vector for N-terminal fusion of 4xHA	Gunnar Schroeder
pUCR6K-miniTn7-Kan	Contains miniTn7-Kan transposon sequence	Robert Heinzen
pTnS2-P1169TnsA-D	Encodes a Tn7 transposase	Robert Heinzen
pUCR6K-miniTn7-Kan-TetRA	Contains anhydrotetracycline-inducible expression cassette in the miniTn7-	This study

	Kan transposon sequence	
pUCR6K-miniTn7-Kan-TetRA-HA-CvpB	Contains anhydrotetracycline-inducible expression cassette of HA-CvpB in the miniTn7-Kan transposon sequence	This study
pUCR6K-miniTn7-Kan-TetRA-4xHA	Contains anhydrotetracycline-inducible expression cassette of 4xHA in the miniTn7-Kan transposon sequence	This study
pUCR6K-miniTn7-Kan-TetRA-4xHA-CvpB	Contains anhydrotetracycline-inducible expression cassette of 4xHA-CvpB in the miniTn7-Kan transposon sequence	This study

370

371

372 **Table 3. List of primers used in this study**

Name	Sequence (restriction sites in bold)
CvpBopt-AgeI-Fw	CTA**ACCGGT**TATGAGTCGCCAGCCAAGTCTG
CvpBopt-BamHI-Rv	CTT**GGATCC**CTTAGTAAAGCTTGCGATTG
PLVX-MluI-NotI-Fw	GTA**ACGCGT**A**GCGGCCGC**GCCACCATGGTGAGCAAGGGC
PLVX-MluI-Rv	CTG**ACGCGT**GACCGGTAGATCCTCTAGTAGAG
CvpBopt-MluI-Fw	GTT**ACGCGT**ATGAGTCGCCAGCCAAG
CvpBopt-NotI-Rv	GAA**GCGGCCGC**TCTTAGTAAAGCTTGCGATTGGC
CvpB-EcoRI-Fw	GAA**GAATTC**AGCAGACAGCCATCATTG
CvpB-SalI-Rv	GAA**GTCGAC**TTACTTAGTGAAAGAAGCAATGG
CvpB1-500-SalI-Rv	GAA**GTCGAC**TTAGTTAAGAGCTTTTCTGGATCCAC
CvpB500-809-EcoRI-Fw	GAA**GAATTC**GGATCCAGAAAAGCTCTTAACG
CvpB-SalI-Fw	CTT**GTCGAC**AGCAGACAGCCATCATTG
CvpB-SphI-Rv	GAA**GCATGC**TTACTTAGTGAAAGAAGCAATGG
CvpBdE-SphI-Rv	GAA**GCATGC**TTATGCGTGAGAGTGACTCTG
2052-SalI-Fw	CTT**GTCGAC**CCTAAAAACACAAATCCAGATC
2052-SphI-Rv	GAA**GCATGC**TTATTTCAAAAAAGCATTTACAAGATC
CvpBopt1-200-NotI-Rv	GAT**GCGGCCGC**TACACTTTTCCATTGAGGC
CvpBopt1-400-NotI-Rv	GAT**GCGGCCGC**TGTTTTCCAGCCCATCAATC
CvpBopt1-500-NotI-Rv	GAT**GCGGCCGC**TATTCAGAGCTTTCCGACTTC
CvpBopt1-600-NotI-Rv	GAA**GCGGCCGC**TCAGCAGATTCTGCATTTCG
CvpBopt100-809-MluI-Fw	GTT**ACGCGT**ATGTACAACGAAAACTTCTACAAGAAGC
CvpBopt200-809-MluI-Fw	GTT**ACGCGT**ATGGCCTCAATGGAAAAGTGTC
CvpBopt400-809-MluI-Fw	GTT**ACGCGT**ATGAAGATTGATGGGCTGGAAAAC
CvpBopt500-809-MluI-Fw	GTT**ACGCGT**ATGCTGATGGCCCGACTGTC
CvpBopt600-809-MluI-Fw	GTT**ACGCGT**ATGATCGAAATGCAGAATCTGC
Cherry-NheI-Fw	GAA**GCTAGC**ATGGTGAGCAAGGGCG
PL17-EcoRI-Rv	GTT**GAATTC**AATGTTCATAATTTTAGCTATTTACATGC
TetR-NheI-Fw	GAGTCA**GCTAGC**TTAAGACCCACTTTCACATTTAAG
TetR-PstI-Rv	GAA**CTGCAG**CTTTTCTCTATCACTGATAG
CvpB-XmaI-Fw	GTT**CCCGGG**TCAGCAGACAGCCATCATTG
CvpB-EcoRI-Rv	GAA**GAATTC**TTACTTAGTGAAAGAAGCAATGG
HA-PstI-Fw	GAA**CTGCAG**ATGTACCCATACGATGTTC
4xHA-PstI-Fw	GAT**CTGCAG**ATGTCAGAAGGAGATATACATATGTAC
4xHA-EcoRI-Fw	CAT**GAATTC**ACGCGTAAATCTTCTCTCATCCGC
Rab5-EcoRI-Fw	CCA**GAATTC**TATGGCTAGTCGAGGCG
Rab5-BamHI-Rv	GGG**GGATCC**TTAGTTACTACAACACTGATTCCTG
Com1-Fw	CGACCGAAGCATAAAAGTCAATG

Com1-Rv	ATTTCATCTTGCTCTGCTCTAACAAC
Com1 Probe	TTATGCGCGCTTTCGACTACCATTTCA

373

374

375 **References**

376

377 1. Martinez E, Cantet F, Fava L, Norville I, Bonazzi M (2014) Identification of
378 OmpA, a *Coxiella burnetii* protein involved in host cell invasion, by multi-phenotypic
379 high-content screening. *PLoS Pathog* 10(3):e1004013–22.

380